

---

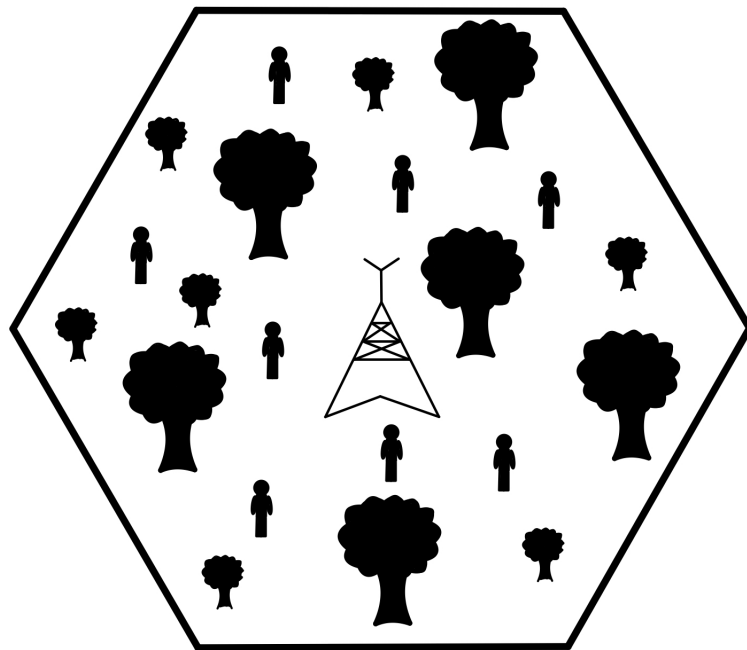
---

# Waveform Design for a Dual-Functional Radar-Communication System

---

---

Bachelor Project  
MatTek6 FrB4211c



Aalborg University  
Mathematics-Technology

Copyright © Aalborg University 2023

This report is written in the typesetting language  $\text{\LaTeX}$  using text editor Overleaf. Experiments and data processing are conducted using Python 3.10.1. Illustrations are created using the TikZ package in  $\text{\LaTeX}$ , Python 3.10.1, or drawn by hand. References are cited using the IEEE method.



# AALBORG UNIVERSITY

## STUDENT REPORT

Department of Mathematical Sciences  
Skjernvej 4A  
DK - 9220 Aalborg  
<http://www.math.aau.dk>

**Title:**

Waveform Design for a Dual-Functional Radar-Communication System

**Theme:**

Bachelor Project

**Project Period:**

Spring Semester 2023

**Project Group:**

MatTek6 FrB4211c

**Participants:**

Christian Dausel Jensen  
Julie Timmermann Werge  
Laurits Randers  
Stine Byrjalsen

**Supervisors:**

Martin Voigt Vejling  
Aysegül Kivilcim  
Petar Popovski

**Page Numbers:** 43**Date of Completion:**

May 24, 2023

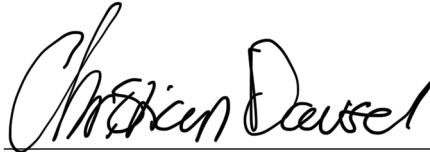
**Abstract:**

This project aims to design a dual-functional waveform with an adjustable trade-off between sensing and communication performance. The focus is on solving the orthogonal Procrustes problem to design the omnidirectional and directional beampatterns, and the trust region subproblem to design a trade-off with a total power constraint. For these designs, numerical experiments are performed for the symbol error probability, detection probability, and signal-to-noise ratio for radar and communication. The results for the omnidirectional and directional beampattern designs show that the choice of the omnidirectional and directional beampatterns depends on the given situation. The results for the trade-off with a total power constraint show that it is possible to adjust the trade-off between radar and communication performance. Thus, the conclusion is that a technique to design a dual-functional waveform with an adjustable trade-off has been developed.

# Preface

This project is written by group FrB4211c in the 6th semester 2023, studying mathematics-technology at the Department of Mathematical Sciences, Aalborg University. The project is written in the period February 1, 2023 to May 24, 2023. The group would like to thank the three supervisors, Martin Voigt Vejling, Aysegül Kivilcim, and Petar Popovski for their guidance throughout the project period. It is expected that the reader has some basic knowledge of probability, statistical processes, and optimisation.

Aalborg University, May 24, 2023



---

Christian Dausel Jensen  
cdje20@student.aau.dk



---

Julie Timmermann Werge  
jwerge20@student.aau.dk



---

Laurits Randers  
lrands18@student.aau.dk



---

Stine Byrjalsen  
sbyrja20@student.aau.dk

# Nomenclature

Acronym	Description
RadCom	Radar-Communication
MIMO	Multiple-Input Multiple-Output
QPSK	Quadratic Phase Shift Keying
SEP	Symbol Error Probability
MUI	Multi-User Interference
SINR	Signal-to-Interference-plus-Noise Ratio
SVD	Singular Value Decomposition
TRS	Trust Region Subproblem
KKT	Karush-Kuhn-Tucker
SNR	Signal-to-Noise Ratio

Notation	Description
$A$ or $a$	Scalar
$\mathbf{a}$	Vector
$\mathbf{A}$	Matrix
$\mathcal{N}$	Normal distribution
$\mathcal{CN}$	Complex normal distribution
$\mathbf{I}_k$	$k \times k$ identity matrix
$j$	Imaginary number
$(\hat{\cdot})$	Estimate
$p$	Probability
$\mathbb{E}$	Expected value
$\ \cdot\ _F$	Frobenius norm
$(\cdot)^H$	Conjugate transpose
$\chi^2$	Chi-square distribution
$\mathbf{1}_k$	All-one vector with $k$ entries
$(\cdot)^T$	Transpose
$(\cdot)_{opt}$	Optimal solution
$\text{Tr}(\cdot)$	Trace
$\overline{(\cdot)}$	Complex conjugate
$\mathcal{L}$	Lagrangian function
$\mathbf{0}_{k \times k}$	$k \times k$ zero matrix
$\text{nullity}(\cdot)$	Dimension of the kernel or null space of a matrix

# Contents

<b>1</b>	<b>Problem Analysis</b>	<b>1</b>
1.1	6G Cellular Networks and its Applications . . . . .	1
1.2	MIMO Systems . . . . .	2
1.3	Dual-Functional Waveform . . . . .	3
1.4	Problem Statement . . . . .	4
1.5	Project Delimitations . . . . .	4
<b>2</b>	<b>Modelling of Communication Systems</b>	<b>5</b>
2.1	Channel Modelling . . . . .	5
2.2	Digital Modulation . . . . .	7
2.3	Symbol Error Probability . . . . .	7
2.4	Power Constraint . . . . .	9
<b>3</b>	<b>Radar Sensing</b>	<b>10</b>
3.1	MIMO Radar . . . . .	10
3.2	Probing Signal Design . . . . .	12
3.3	Detection Probability . . . . .	14
<b>4</b>	<b>Optimisation Methods</b>	<b>17</b>
4.1	Orthogonal Procrustes Problem . . . . .	17
4.2	Trust Region Subproblem . . . . .	18
<b>5</b>	<b>Waveform Design</b>	<b>22</b>
5.1	Omnidirectional Beampattern Design with a Strict Equality Constraint . . . . .	22
5.2	Directional Beampattern Design with a Strict Equality Constraint . . . . .	23
5.3	Trade-off Design with a Total Power Constraint . . . . .	24
<b>6</b>	<b>Numerical Results</b>	<b>28</b>
6.1	Omnidirectional and Directional Beampatterns with Strict Equalities . . . . .	28
6.2	Trade-off with a Total Power Constraint . . . . .	32
<b>7</b>	<b>Discussion</b>	<b>38</b>
<b>8</b>	<b>Conclusion</b>	<b>39</b>
	<b>Bibliography</b>	<b>40</b>
<b>A</b>	<b>Linear Algebra</b>	<b>42</b>

# 1 Problem Analysis

Today, radar and wireless communication are widely used around the world separately. Radar is used to measure physical data, such as location and velocity, while wireless communication is used to transfer information over short and long distances. 6G is the sixth generation of wireless technology, and it is expected to launch in 2030 [4, p. 562]. Dual-functional radar-communication (RadCom) will be a key feature in 6G. The history of dual-functional RadCom dates back to 1963, where the first signalling scheme on the subject was proposed [12, p. 1729]. Dual-functional RadCom leads to mutual performance gains such as communication-assisted sensing and sensing-assisted communication. Communication-assisted sensing is utilising the information that the communication system provides. An example of this could be to estimate the distance to a target by measuring the signal strength. Hence, the system can achieve better sensing performance than if it relied solely on traditional sensing techniques. The idea is the same with sensing-assisted communication, where the information provided by the sensing system is used in order to improve the communication system. For instance, beamforming can be enhanced in communication by using the location of the user from the sensing system.

The application of dual-functional RadCom is beneficial in, among other things, smart home features, healthcare, and autonomous vehicles. Merging radar and communication into a single system also reduces hardware and signalling costs. However, there can be some challenges of merging radar and communication. One of the challenges is to design a dual-functional waveform that can be used for both sensing and communication. There are two main approaches to this design: non-overlapped resource allocation or fully unified waveforms. In the first case, the wireless resources are scheduled to not interfere with each other. In the second case, sensing is implemented in an already existing communication system, or vice versa. However, the fully unified waveforms also approach a joint design where a trade-off between sensing and communication is obtainable. The non-overlapping waveforms are easier to implement since they can be designed such that they do not interfere with each other. However, this design has the disadvantages of low spectral and energy efficiency. The fully unified waveforms using a joint design are the most preferable method since they entail a scalable sensing and communication performance trade-off. This design can be obtained by solving a non-convex optimisation problem. Such a problem can be solved using the orthogonal Procrustes or the trust region subproblem method [12, p. 1748]. In order to understand the theory behind dual-functional RadCom, some basic knowledge of cellular networks is needed.

## 1.1 6G Cellular Networks and its Applications

A cellular network is a communication network that is divided into areas, or cells. These cells are often hexagonal since they provide the best coverage with limited dead spots. Each cell has a base station, which is a fixed-location transceiver that can both transmit and receive communication via antennas. To avoid interference within each cell, a cell uses a different set of frequencies than its neighbouring cells [16, pp. 341–342]. A cellular

## 1.2. MIMO Systems

network can be seen in Figure 1.1.

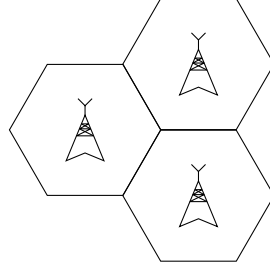


**Figure 1.1:** A cellular network with three cells.

Rising demands for higher data rates and greater network capacity has led to the evolution of existing cellular network architectures. This is a reason behind the development of 6G technology, which builds on the principles of the existing cellular network architecture. Each cell from Figure 1.1 remains the same in 6G, but with additional capabilities and improvements such as higher data rates, lower latency, and higher frequency bandwidths [26, pp. 8–10]. The increased frequencies and bandwidth will occur somewhere in the terahertz (THz) gap at a frequency between 100 GHz and 10 THz, which is higher than the current frequencies used for 5G. This is desirable because more bandwidth corresponds to a higher maximum rate of data transfer [26, pp. 17–18].

In 6G, both sensing and communication will play an important role. Since both radar and communication systems are evolving towards higher frequency bands and larger antenna arrays, they are becoming increasingly similar. Therefore, combining them leads to a single system, 6G. This allows for new applications in areas such as autonomous driving. An autonomous car collects an enormous amount of data that must be shared, for example, to inform other road users of its position. The car must also react autonomously to unforeseen circumstances with extremely low latency. Therefore, a very high data rate and low latency are required at the same time, which could be possible with 6G [26, pp. 10–11, 14]. Another use for 6G could be in the field of monitoring drones. The use of drones in civilian applications has increased in the last few years. This creates problems since drones have the potential to be used in no-fly zones or in illegal activities, such as the surveillance of objects and individuals. Since drones are small, vary in shape, and fly at low altitudes, they are difficult to detect with other surveillance technologies. Here, the use of sensing would provide a solution to monitor non-cooperative drones in low-altitude airspace [12, pp. 1733–1734].

## 1.2 MIMO Systems

In this project, we consider a multiple-input multiple-output (MIMO) system with multiple antennas at the transmitter, also referred to as the base station, and a single antenna at each receiver. A MIMO communication system uses multiple antennas in order to transmit and receive multiple versions of the same signal. These versions originate from the transmit antennas but as they traverse through different propagation paths within the environment



### 1.3. Dual-Functional Waveform

they undergo different changes. Therefore, they can be thought of as different versions of the original signal. Also, the environment is referred to as the channel. The channel can consist of two or more paths, which results in the signals being phase shifted when arriving at the receiver. This is known as multipath propagation. The receiver is designed to take multipath propagation into account such that it can recombine the data structure. Therefore, if one receiver is experiencing strong destructive interference, another is likely to obtain a sufficient signal. Thus, MIMO systems reduce issues such as fading, which is the attenuation of the signal power while it travels through the channel. In other words, MIMO exploits multipath propagation. This method is a form of spatial diversity, which means that the wireless channel model uses two or more antennas at the base station to improve the signal quality [16, pp. 284, 316–317].

A MIMO radar system corresponds to a standard phased-array radar, but with more capabilities. A phased-array is an improved simple antenna array, which is an antenna that pulsates radio waves in a fixed direction. The phased-array can steer the direction of the beam of radio waves without physically moving the antennas. The MIMO radar can use the transmitted vector to design a superior beampattern compared to the phased-array due to the increased number of degrees of freedom, which at minimum corresponds to the number of antennas. Furthermore, MIMO radar minimises the cross-correlation of the signals reflected from the targets of interest [10, pp. 1–3].

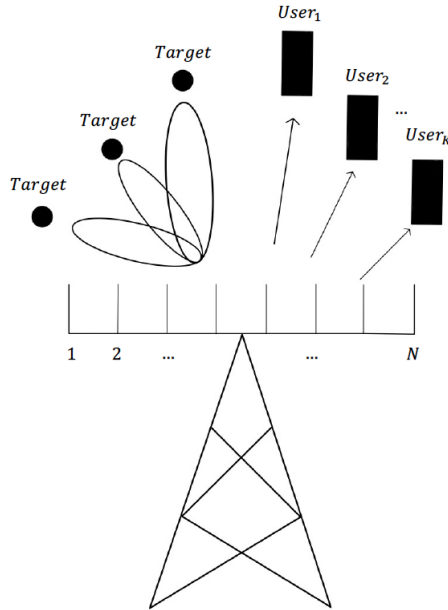


Figure 1.2: Dual-functional MIMO RadCom System.

### 1.3 Dual-Functional Waveform

As stated before, the higher frequency bands and larger antenna arrays of the radar and communication systems are leading to similar channel characteristics. Therefore, it is achievable to design a waveform for the dual-functional MIMO RadCom system which

#### 1.4. Problem Statement

simultaneously transmits radar waveforms to the targets of interest and communicates to the users, as seen in Figure 1.2 [13, p. 4266]. However, a base station has limited resources in terms of transmit power and the number of antennas. Hence, when a dual-functional waveform is used, the resources have to be shared between sensing and communication. The resources can be allocated differently, depending on the situation. The distribution could be evenly divided between sensing and communication or heavily skewed towards either. For instance, in a scenario where the system encounters a greater number of targets than users, a minimum level of communication is required, hence, resources might be dedicated to sensing. Conversely, the resources can be dedicated to communication if desired. The balance of designating the resources is referred to as an adjustable trade-off. The necessity for trade-off arises because the requirements for optimal radar performance often conflict with those for optimal communication performance. The conflict primarily arises due to the radar and communication counteracting beamforming. Radar systems prefer to concentrate energy towards potential targets to maximise detection. On the other hand, communication systems tends to distribute energy towards users to ensure connectivity [13, pp. 4264–4265]. Hence, it is necessary to design a dual-functional waveform with an adjustable trade-off between sensing and communication performance. This leads to the following problem statement.

#### 1.4 Problem Statement

*"How can a dual-functional waveform be designed with an adjustable trade-off between sensing and communication performance?"*

#### 1.5 Project Delimitations

To achieve the problem statement, we aim to design a waveform that provides an adjustable trade-off between the sensing and communication performance. Focus will be on solving certain optimisation problems to design the waveform.

We consider a system that has  $N$  evenly spaced antennas at the base station, which serve dual roles as transmitters of the waveform and receivers of the radar signal. The system simultaneously serves  $K$  single-antenna users and senses targets. We assume that there are more antennas than users,  $K < N$  [2, p. 369]. For simplicity the waveform is modelled using a narrowband model. The radar system is not able to estimate the distances to the targets, due to a lack of one degree of freedom. Therefore, the targets and users are assumed to have a known distance from the base station. Since our main objective is to design a dual-functional waveform, our interest lies only in estimating the angle to the target.

Regarding the communication channel, we assume Rayleigh fading, which remains unchanged in a single communication frame. In addition, we assume that the base station can perfectly estimate the channel [13, p. 4266].

## 2 Modelling of Communication Systems

In this chapter a model of narrowband wireless communication is presented. The concepts of large-scale and small-scale fading will be introduced, which are two types of fading that are considered when modelling wireless channels. Furthermore, Rayleigh fading will be presented. Then it will be discussed how the channel can be modelled as a sum of all the reflections and how small-scale fading occurs when the signal propagates through different paths between the transmitter and receiver. Lastly, a digital modulation technique and a measure of communication performance is reviewed.

The signal at the receiver can be modelled as a linear system with additive noise [20, p. 41]. As mentioned in Section 1.5, we consider a MIMO system with  $N$  transmit antennas, serving  $K$  single-antenna receivers. The signal at the single receiver is then given by

$$\mathbf{y}_{com} = \mathbf{H}\mathbf{x} + \mathbf{w},$$

where  $\mathbf{y}_{com} \in \mathbb{C}^K$  is the signal at the receivers,  $\mathbf{x} \in \mathbb{C}^N$  is the signal sent by the transmitter,  $\mathbf{H} \in \mathbb{C}^{K \times N}$  is the channel matrix, and  $\mathbf{w} \in \mathbb{C}^K$  is additive white complex Gaussian noise  $\mathbf{w} \sim \mathcal{CN}(0, N_0 \mathbf{I}_K)$ . The noise is generated by the receiver amplifier and external radio interference [20, pp. 41–42].

In wireless communication, it is common to split the transmission into segments of time called frames. In this project, we assume that in a frame, the transmitter makes  $L$  transmissions to the receivers. This can be formulated as

$$\mathbf{Y}_{com} = \mathbf{H}\mathbf{X} + \mathbf{W},$$

where  $\mathbf{Y}_{com} = [\mathbf{y}_1 \ \mathbf{y}_2 \ \dots \ \mathbf{y}_L] \in \mathbb{C}^{K \times L}$  is the received symbol matrix, where a symbol is one or more bits determined by a modulation format. Furthermore,  $\mathbf{X} = [\mathbf{x}_1 \ \mathbf{x}_2 \ \dots \ \mathbf{x}_L] \in \mathbb{C}^{N \times L}$  is the transmitted signal matrix,  $\mathbf{H} = [\mathbf{h}_1 \ \mathbf{h}_2 \ \dots \ \mathbf{h}_K]^T \in \mathbb{C}^{K \times N}$  is the channel matrix, and  $\mathbf{W} = [\mathbf{w}_1 \ \mathbf{w}_2 \ \dots \ \mathbf{w}_L] \in \mathbb{C}^{K \times L}$  is the noise matrix where  $\mathbf{w}_i \sim \mathcal{CN}(0, N_0 \mathbf{I}_K)$  for  $i = 1, \dots, L$  [13, p. 4266]. In order to analyse and simulate a wireless communication system, a mathematical model of the channel is needed.

### 2.1 Channel Modelling

The channel of a communication system was described as the environment the signals travel through in Section 1.2, but to be more precise, the channel is a medium or a pathway. In common outdoor settings, the pathway between the transmitter and receiver is full of objects that affect the propagation of the signal. The channel effects are summarised into three mechanisms: reflection, diffraction, and scattering. Reflection occurs when the wave strikes an object, where some of the wave energy is absorbed by the object, known as shadowing. Furthermore, the wave is reflected in another direction. Diffraction is a

## 2.1. Channel Modelling

phenomenon where the wave bends around the edges of objects. Scattering occurs when the wave hits a surface and the energy of the wave is spread into multiple propagating waves. The combination of these effects leads to a simplification of the term attenuation of the signal. In other words, the channel effects are what cause fading [16, pp. 4–5].

When modelling wireless channels, two types of fading are considered:

- *Large-scale fading* is when the signal power is attenuated due to travelling large distances, this is called path loss, and large objects such as hills and buildings blocking the signal. This usually occurs when the receiver is far away from the transmitter. In the context of cell phones, this is, for instance, when a phone communicates with a base station in a neighbouring cell.
- *Small-scale fading* is due to constructive and destructive interference when the signal propagates through different paths. The signal undergoes multipath propagation as a result of being reflected and scattered when hitting a surface. This is more prominent when the cell phone and base station are within the same cell.

Due to the assumption of a small distance between the transmitter and receiver, only small-scale fading is considered. The signal at the receiver can be modelled as the sum of all the reflections. Therefore, the channel between the  $m$ th antenna and the  $i$ th user is given by

$$H_{i,m} = \sum_{c=0}^C a_c e^{-j2\pi f_0 \tau_c}, \quad (2.1)$$

where  $f_0$  is the carrier frequency,  $C$  is the number of reflections,  $a_c$  is the attenuation of the  $c$ th reflection, and  $\tau_c$  is the propagation delay of the  $c$ th reflection. If each reflection attenuation and propagation delay are assumed to be independent, then (2.1) becomes a sum of independent random variables. In small-scale fading, a large number of reflections occur, and it is assumed this tends to infinity. Due to the central limit theorem, as the number of paths tends to infinity  $H_{i,m} \sim \mathcal{CN}(0, \sigma_H^2)$ . This is called Rayleigh fading [20, pp. 47–48]. Furthermore, small-scale fading can be classified into two types: flat fading or frequency-selective fading. Flat fading means that the fading is frequency-flat, hence, all frequencies in the signal are attenuated equally in the frequency band. Frequency-selective fading means that the attenuation of all frequencies varies significantly across the frequency range [20, p. 45].

The fading of this project is assumed to be flat Rayleigh fading. In a flat Rayleigh fading channel, the attenuation of the signal varies randomly with time, causing the amplitude and phase of the received signal to swing rapidly. However, it can be assumed that the channel is constant for a certain amount of time. This is called coherence time. Due to the rapid and random attenuation over time, the coherence time is relatively small. Therefore, the time it takes the transmitter to transmit one symbol can be assumed to be larger than the coherence time. Hence, the entries in the channel matrix  $\mathbf{H}$  are independent, also called noncoherent communication [20, pp. 27, 64–65].

## 2.2 Digital Modulation

In order to transmit digital information, it has to be converted from bits into an analogue waveform, which is transmitted over the channel. This is accomplished by digital modulation, which encodes digital information into the transmitted signal. Digital modulation uses various techniques to alternate the amplitude, frequency, and phase of the transmitted signal. An example is the technique called quadratic phase shift keying (QPSK), which solely alternates the phase of the transmitted signal. QPSK is a bits-to-symbols mapping, which means it maps a pair of bits on the unit circle in the complex plane. The unit circle consists of four points that are equidistantly located  $\frac{\pi}{2}$  apart from each other. These points are called constellation symbols, and the map is called a constellation diagram. QPSK can thus assign a sequence of bits to the carrier signal by modulating its phase [8, pp. 14–15]. This is depicted on Figure 2.1a and Figure 2.1b.

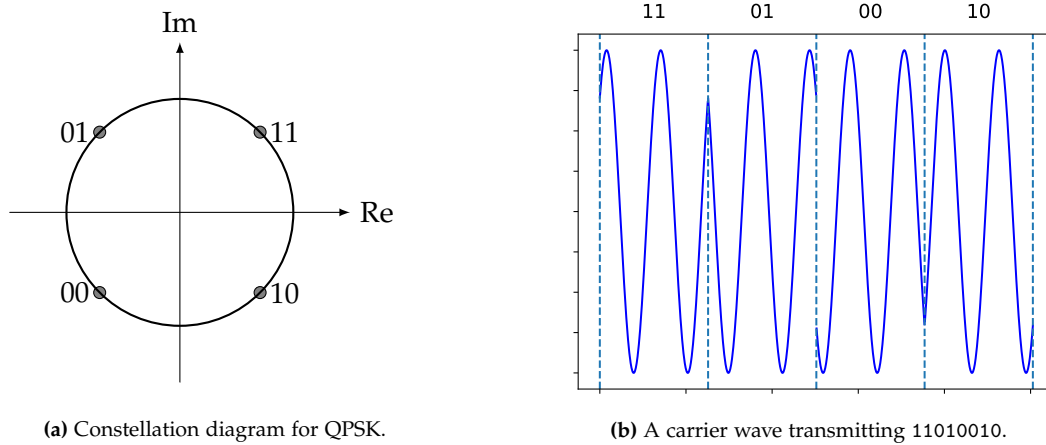


Figure 2.1

The constellation mapping by QPSK is usually done by Gray encoding, also called Gray code. This means that the symbols adjacent to each other do not differ by more than one bit. This property makes Gray encoding particularly useful in situations where noise or interference causes errors in the received signal. In contrast, if a binary encoding were used, adjacent symbols in the constellation diagram could differ by more than one bit, increasing the number of bit errors [8, p. 15].

## 2.3 Symbol Error Probability

The symbol error probability (SEP) measures the probability that a symbol is incorrectly detected or received in the presence of noise in the communication channel. This will be used as a measure of communication performance. In QPSK, there are four decision regions, which correspond to the four possible transmitted symbols. Furthermore, the decision regions correspond to the areas in the constellation diagram where the received signal points are closest to one of the four transmitted symbols. The decision regions can

### 2.3. Symbol Error Probability

be defined by a function  $d(\cdot)$ :

$$\hat{s} = d(y),$$

where  $d(\cdot)$  maps the received symbol  $y$  to the closest symbol,  $\hat{s}$  is the estimate of the transmitted symbol obtained from the decision function. The SEP is the probability of decoding a symbol wrong and is defined as

$$P_e = p(\hat{s} \neq s | s \text{ transmitted}),$$

where  $s$  is the true value of the symbol [16, p. 114].

It is desirable to achieve a lower SEP since it implies that the receiver is more likely to correctly decode the received symbols. This can be problematic due to the multi-user interference (MUI) that can increase the SEP for each user. To describe the effect of MUI, the received signal can be expressed in terms of a desired constellation symbol matrix  $\mathbf{S} \in \mathbb{C}^{K \times L}$ . Specifically, the signal at the receivers can be represented as

$$\mathbf{Y}_{com} = \mathbf{S} + \mathbf{H}\mathbf{X} - \mathbf{S} + \mathbf{W}.$$

The term  $\mathbf{H}\mathbf{X} - \mathbf{S}$  is referred to as the MUI signal. This represents interference that occurs when communicating with multiple users simultaneously. Since communication happens simultaneously, one receiver also obtains the signals intended for the other receivers, hence, interference occurs [13, p. 4266].

When analysing a wireless communication system with multiple users, one important metric is the signal-to-interference-plus-noise ratio (SINR). The SINR is used to measure the channel quality for each user. It is defined as the ratio between the power of the signal and MUI energy for the user plus background noise. The SINR for the  $i$ th user is given by

$$\gamma_i = \frac{\mathbb{E}(|s_{i,t}|^2)}{\mathbb{E}(|\mathbf{h}_i^T \mathbf{x}_t - s_{i,t}|^2) + N_0},$$

where  $\mathbb{E}$  denotes the expected value with respect to the time index  $t$ . The  $|s_{i,t}|^2$  term is the power of the signal intended for the  $i$ th user, while in the denominator  $|\mathbf{h}_i^T \mathbf{x}_t - s_{i,t}|^2$  represents the power of the interference at the  $i$ th user. Lastly,  $N_0$  is the variance of the noise.

The SINR can be maximised by minimising the total MUI energy, which is given by

$$P_{\text{MUI}} = \|\mathbf{H}\mathbf{X} - \mathbf{S}\|_F^2.$$

This leads to the connection between the SEP and SINR. The probability of a symbol error occurring is dependent on the quality of the channel, in other words, if the channel is noisy, the SEP will be increased [20, pp. 17–18]. Hence, given a constellation and channel matrix, the desired waveform can be designed by minimising the MUI energy [13, p. 4266] [15, p. 1060].

## 2.4 Power Constraint

The transmitter cannot transmit a signal with infinite power. Hence, when designing a waveform, the total power has to be constrained. The total power the system can transmit is assumed to be known and is denoted  $P_T$ . In this project, two different power constraints are considered: the per-antenna power constraint and the total power constraint. The per-antenna power constraint is where the transmitter transmits with equal power on all the antennas. This constant is equivalent to

$$\frac{1}{L} \text{diag}(\mathbf{X}\mathbf{X}^H) = \frac{P_T}{N} \mathbf{1}_N,$$

where  $\text{diag}(\cdot)$  constructs a vector of the diagonal entries of a matrix and  $\mathbf{1}_N = [1 \ 1 \ \dots \ 1]^T \in \mathbb{R}^N$ . The total power constraint is where only the total transmitted power is constrained. Mathematically, this is given as

$$\frac{1}{L} \|\mathbf{X}\|_F^2 = P_T.$$

In general, the per-antenna power constraint is considered more strict [15, p. 1060].

### 3 Radar Sensing

A radar is a system for detection and localisation of objects using radio waves. A radio wave is an electromagnetic wave with frequencies up to 300 GHz in the electromagnetic spectrum [24, p. 436]. The radio waves are emitted by the transmitting antenna. When the radio wave hits a target, it is reflected back to the receiving antenna. If the transmitting and receiving are performed by the same antenna, the radar system is called monostatic. Otherwise, it is called bistatic. A monostatic radar system can be seen in Figure 3.1.

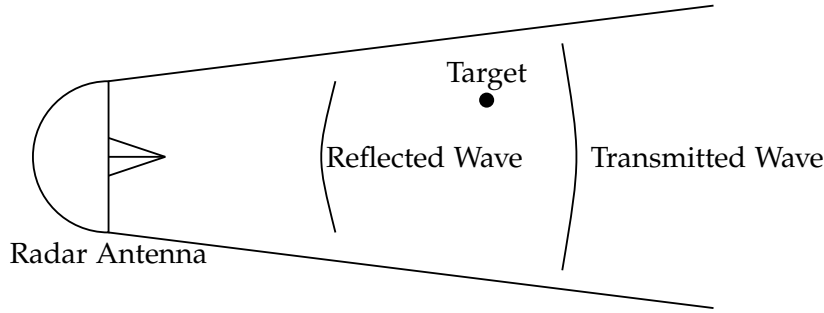


Figure 3.1: A monostatic radar system.

From the receiving antenna, the signal is delivered to a receiver, where the state of the target is extracted. This could, for example, be information of the location and velocity of the target [19, p. 1]. Multiple antennas connected together to work as one single antenna are called an antenna array. A phased array is an antenna array where each individual antenna element can have different phase shifts. This is controlled by a computer without the antennas moving physically. The benefit of a phased array is being able to steer the radio waves in different directions. An advanced type of phased array is a MIMO radar. A standard phased array transmits scaled versions of a single waveform, whereas a MIMO radar can transmit multiple probing signals simultaneously [10, pp. 1–3].

#### 3.1 MIMO Radar

Consider a MIMO radar system with  $N_T$  transmit antennas and  $N_R$  receive antennas. A MIMO radar can identify a maximum number of targets up to  $N_T$  times that of its phased-array counterpart [10, p. 2]. The transmit signal vector is given as

$$\mathbf{x}(n) = [x_1(n) \ x_2(n) \ \cdots \ x_{N_T}(n)]^T \quad \text{for } n = 1, \dots, L$$

where  $x_m(n)$  is the discrete-time baseband signal transmitted by the  $m$ th transmit antenna. The array for the transmit antenna is described by the steering vector. The steering vector represents the phase delays for an incoming wave at each antenna. For a uniform linear array the steering vector is

$$\mathbf{a}(\theta_t) = \left[ 1 \ e^{-j2\pi \frac{d}{\lambda} \sin(\theta_t)} \ \cdots \ e^{-j2\pi \frac{d}{\lambda} \sin(\theta_t)(N_T-1)} \right]^T, \quad (3.1)$$



### 3.1. MIMO Radar

where  $\theta_t$  is the departure angle,  $\lambda$  is the wavelength of the transmitted signal, and  $d$  is the distance between the antennas as depicted in Figure 3.2.

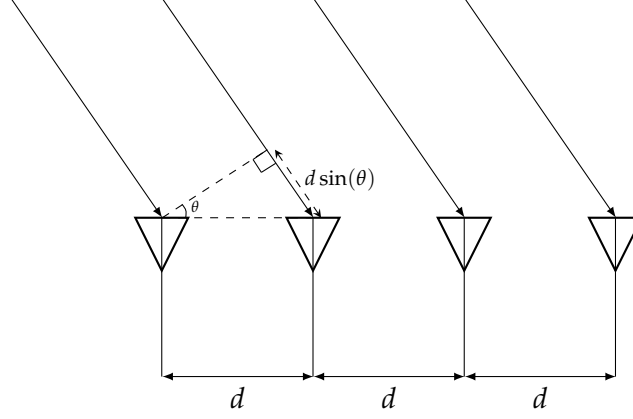


**Figure 3.2:** Uniform linear array antennas.

In a uniform linear array, the spacing  $d$  between the antennas is uniform. When the spacing is equal to or greater than half of the wavelength, multiple side lobes will be formed. Therefore, to achieve a higher directivity for the antenna array, the spacing is set equal to  $d = \frac{\lambda}{2}$  [6, pp. 1–2]. This yields the following expression for (3.1)

$$\mathbf{a}(\theta_t) = [1 \quad e^{-j\pi \sin(\theta_t)} \quad \dots \quad e^{-j\pi \sin(\theta_t)(N_T-1)}]^T.$$

The received signal is given as

$$\mathbf{y}(n) = [y_1(n) \quad y_2(n) \quad \dots \quad y_{N_R}(n)]^T \quad \text{for } n = 1, \dots, L$$

where  $y_m(n)$  is the signal received by the  $m$ th receive antenna. The array for the receive antenna is described by the steering vector

$$\mathbf{a}(\theta_r) = [1 \quad e^{-j\pi \sin(\theta_r)} \quad \dots \quad e^{-j\pi \sin(\theta_r)(N_R-1)}]^T,$$

where  $\theta_r$  is the arriving angle at the receive antenna [24, p. 439]. The received data vector with  $B$  paths is then

$$\mathbf{y}(n) = \sum_{b=1}^B \beta_b \mathbf{a}(\theta_{r,b}) \mathbf{a}^T(\theta_{t,b}) \mathbf{x}(n) + \epsilon(n), \quad (3.2)$$

where  $\beta_b$  is the complex channel gain and  $\epsilon(n)$  is additive white complex noise  $\epsilon(n) \sim \mathcal{CN}(0, \sigma_\epsilon^2 \mathbf{I}_{N_R})$  [27, p. 2].

The complex channel gain can be written as

$$\beta_b = |\beta_b| e^{j \frac{2\pi(d_{1,b} + d_{2,b})}{\lambda}},$$

where  $d_{1,b}, d_{2,b}$  are the lengths of the paths from the antenna to the object causing scattering and from that to the target. If the wavelength is large compared to the distance to

### 3.2. Probing Signal Design

the object, a small change in position results in a large difference in phase. Hence, it is reasonable to assume that the phase of the channel gain is uniformly distributed on the interval 0 to  $2\pi$ . The amplitude is a function of how well the object is reflecting the signal and the path loss. It is assumed that the amplitude is normal distributed. Hence, the complex channel gain can be modelled as  $\beta_b \sim \mathcal{CN}(0, \sigma_{\beta_b}^2)$  [7, p. 7584] [1, p. 4947].

As specified in Section 1.5, we assume the radar system to be monostatic. Therefore, the number of transmit antennas  $N_T$  and receive antennas  $N_R$  are the same number of antennas, is denoted as  $N$ . The same applies to the angles  $\theta_t$  and  $\theta_r$ , which will be denoted as  $\theta$ .

## 3.2 Probing Signal Design

The radar beampattern can be designed to concentrate power towards desirable directions to increase the chance of detecting a target. The desired beampattern can be obtained by designing the probing signal. The power of the probing signal, also called the transmit beampattern, transmitted from the antenna at an angle  $\theta$ , is given by

$$P(\theta) = \mathbf{a}^H(\theta) \mathbf{R} \mathbf{a}(\theta),$$

where  $\mathbf{R}$  is the covariance matrix of the transmit signal vector  $\mathbf{x}(n)$ , defined as

$$\mathbf{R} = \mathbb{E}[\mathbf{x}(n) \mathbf{x}^H(n)]. \quad (3.3)$$

However, (3.3) is a theoretical covariance matrix, which cannot be exactly determined. Hence, in practice, an estimate is used instead, the sample covariance matrix, defined as

$$\hat{\mathbf{R}} = \frac{1}{L} \mathbf{X} \mathbf{X}^H,$$

where  $\mathbf{X} \in \mathbb{C}^{N \times L}$  is the transmitted signal matrix [9, pp. 70–72] [13, p. 4266]. Since the transmitter cannot transmit a signal with infinite power, the covariance matrix has to be chosen under a per-antenna power constraint

$$\hat{R}_{mm} = \frac{P_T}{N}, \quad m = 1, \dots, N,$$

where  $\hat{R}_{mm}$  denotes the  $(m, m)$ th entry of  $\hat{\mathbf{R}}$ ,  $N$  is the number of transmit antennas, and  $P_T$  is the total transmit power.

With the design of  $\hat{\mathbf{R}}$  under the per-antenna power constraint, it is desired to achieve the following goals:

- a) To approximate or match a desired transmit beampattern, and
- b) to minimise the cross-correlation between the probing signals at a number of given target locations.

### 3.2. Probing Signal Design

According to (a), it is desired to choose  $\hat{\mathbf{R}}$  such that the transmit power is used to maximise the probing signal power at the locations of the targets of interest and to minimise it anywhere else. Regarding (b), the cross-correlation between the probing signals at the angles  $\theta_1$  and  $\theta_2$  is defined as

$$\mathbf{a}^H(\theta_1)\hat{\mathbf{R}}\mathbf{a}(\theta_2).$$

Choosing  $\hat{\mathbf{R}}$  depends on the considered MIMO design problem. In this project,  $\hat{\mathbf{R}}$  is chosen as the covariance matrix  $\hat{\mathbf{R}} \in \mathbb{R}^{N \times N}$ , which can be defined as

$$\hat{\mathbf{R}} = \frac{P_T}{N} \begin{bmatrix} 1 & \zeta & \zeta^2 & \dots & \zeta^{N-1} \\ \zeta & 1 & \zeta & \ddots & \vdots \\ \zeta^2 & \zeta & 1 & \ddots & \\ \vdots & \ddots & \ddots & \ddots & \zeta \\ \zeta^{N-1} & \dots & \zeta & 1 & \end{bmatrix},$$

where  $0 \leq \zeta \leq 1$ . In the case of orthogonal transmit signals, i.e.,  $\zeta = 0$ , the signals are mutually uncorrelated, and the covariance matrix is  $\hat{\mathbf{R}} = \frac{P_T}{N} \mathbf{I}_N$ . This results in an omnidirectional transmission, which is the transmission of radio waves equal in all directions. In the case where  $\zeta = 1$ , the signals are perfectly coherent. For values of  $\zeta$  between 0 and 1, the signals are partially correlated. This results in a directional transmission, which focuses the transmission in a certain number of directions based on the number of antennas [18, pp. 173–174]. On Figure 3.3, the beampattern is shown for different values of  $\zeta$ . It can be seen that for  $\zeta = 0$  the beampattern is omnidirectional and becomes more concentrated at  $\theta = 0^\circ$  as  $\zeta$  increases.

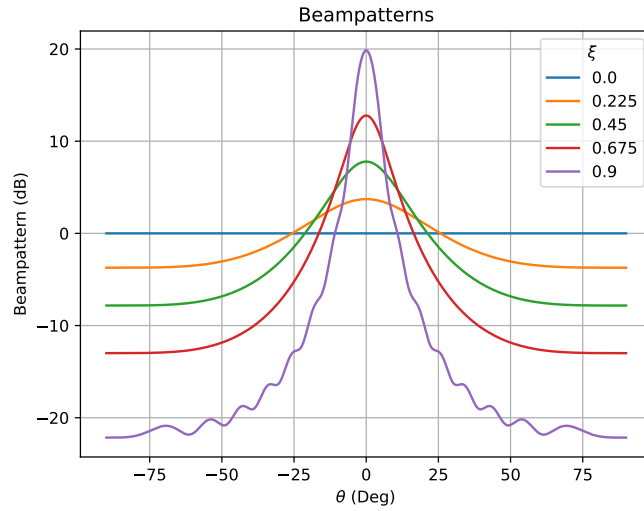


**Figure 3.3:** Beampatterns for different values of  $\zeta$ .  $P_T = 1$  and  $N = 16$ .

### 3.3 Detection Probability

In target detection, the target is either present or absent. If it is present, the received waveform is reflected by the target with some additive noise due to the electronic components and external sources. If the target is absent, only noise will be present. Thus, to measure the performance of the radar system, it is desired to distinguish between a present or absent target. This can be modelled as a hypothesis testing problem, where the two hypotheses  $\beta \neq 0$  and  $\beta = 0$  are when the target is present or absent, respectively. If  $\beta \neq 0$  holds true and the target is detected, it is referred to as the probability of detection, denoted  $P_D$ . If  $\beta = 0$  holds true but a target is detected, a false alarm occurs. The probability of a false alarm is denoted  $P_{FA}$ . False alarms are generated when noise exceeds a chosen threshold level, denoted  $\gamma$ . If the threshold is too low, the number of false alarms increases, masking the detection of real targets. If the threshold is too high, fewer targets and false alarms will be detected. Therefore, a balanced threshold level is desired.

In this project, our aim is to compute the detection probability of a target along a hypothesised path. This is done by following the derivation in [27, p. 3]. If the number of receive antennas or the signal bandwidth go to infinity, the paths are independent and the resolution is high enough to distinguish one target from another. However, as it is customary to have large antenna arrays, it is assumed that the paths are always independent [1, p. 4943]. Hence, only one path is observed. Thus, we will restate the received data vector (3.2) for  $B = 1$ , and define the hypothesised received data vector as

$$\tilde{\mathbf{y}}(n) = \tilde{\beta} \mathbf{a}(\tilde{\theta}) \mathbf{a}^T(\tilde{\theta}) \mathbf{x}(n) + \epsilon(n),$$

where  $\epsilon(n) \sim \mathcal{CN}(0, \sigma_\epsilon^2 \mathbf{I}_N)$  and  $\tilde{(\cdot)}$  represent the hypothesised value.

The detection probability for  $\tilde{\mathbf{y}}(n)$  is calculated using the following method. First,  $\tilde{\mathbf{y}}(n)$  must separate the components stemming from the target and noise. Then, the signal is normalised to obtain the scalar value,  $\tilde{y}$ . From this we derive  $|\tilde{y}|^2$  as our test statistic of interest which has a non-central  $\chi^2$  distribution. The distribution of the test statistic allows us to calculate the  $P_D$  [27, p. 3].

First, a matched filter is used, thus multiplying  $\tilde{\mathbf{y}}(n)$  with the conjugate transpose of  $\tilde{\mathbf{p}}(n) = \mathbf{a}(\tilde{\theta}) \mathbf{a}^T(\tilde{\theta}) \mathbf{x}(n)$ , yielding

$$\tilde{z}(n) = \tilde{\beta} \|\tilde{\mathbf{p}}(n)\|^2 + \tilde{\mathbf{p}}(n)^H \epsilon(n).$$

This is done since  $\tilde{\mathbf{p}}(n)$  is a known transmitted signal, where the unknown reflected signal  $\tilde{\mathbf{y}}(n)$  is examined for the elements that match those of the transmitted signal [21, p. 313]. When multiplying  $\epsilon(n)$  with  $\tilde{\mathbf{p}}(n)^H$  the variance changes to  $\|\tilde{\mathbf{p}}(n)\|^2 \sigma_\epsilon^2$ . Furthermore, when a constant is added to  $\epsilon(n)$ , the mean and variance are shifted, hence, the distribution is  $\tilde{z}(n) \sim \mathcal{CN}(\tilde{\beta} \|\tilde{\mathbf{p}}(n)\|^2, \|\tilde{\mathbf{p}}(n)\|^2 \sigma_\epsilon^2)$ .

Then, the observation  $\tilde{y}$  is defined as the sum of  $\tilde{z}(n)$  over all transmissions, such that

$$\tilde{y} = \sum_{n=1}^L \tilde{z}(n).$$

### 3.3. Detection Probability

The normalisation of  $\tilde{y}$  can be calculated as

$$\check{y} = \frac{\tilde{y}}{\sqrt{\text{var}(\tilde{y})/2}},$$

where  $\tilde{y} \sim \mathcal{CN}\left(\sigma_\epsilon^2 \tilde{\beta} \sum_{n=1}^L \|\tilde{\mathbf{p}}(n)\|^2, 2\right)$ . The test statistic of interest is  $|\check{y}|^2 = \text{Re}\{\check{y}\}^2 + \text{Im}\{\check{y}\}^2$ . Since

$$\begin{aligned} \text{Re}\{\check{y}\}^2 &\sim \mathcal{N}\left(\sigma_\epsilon^2 \tilde{\beta} \sum_{n=1}^L \|\tilde{\mathbf{p}}(n)\|^2, 1\right), \\ \text{Im}\{\check{y}\}^2 &\sim \mathcal{N}\left(\sigma_\epsilon^2 \tilde{\beta} \sum_{n=1}^L \|\tilde{\mathbf{p}}(n)\|^2, 1\right), \end{aligned}$$

then  $|\check{y}|^2$  follows a non-central  $\chi^2$  distribution with two degrees of freedom, denoted  $|\check{y}|^2 \sim \chi_2^2(\lambda)$ . The non-centrality parameter  $\lambda$  is the sum of the squared expected value of  $\text{Re}\{\check{y}\}$  and  $\text{Im}\{\check{y}\}$ , hence

$$\begin{aligned} \lambda &= \mathbb{E}[\text{Re}\{\check{y}\}]^2 + \mathbb{E}[\text{Im}\{\check{y}\}]^2 \\ &= |\mathbb{E}[\check{y}]|^2 \\ &= \left| \frac{\sum_{n=1}^L \tilde{\beta} \|\tilde{\mathbf{p}}(n)\|^2}{\frac{\sqrt{\sigma_\epsilon^2 \sum_{n=1}^L \|\tilde{\mathbf{p}}(n)\|^2}}{\sqrt{2}}} \right|^2 \\ &= \frac{2|\tilde{\beta}|^2}{\sigma_\epsilon^2} \frac{|\sum_{n=1}^L \|\tilde{\mathbf{p}}(n)\|^2|^2}{\sum_{n=1}^L \|\tilde{\mathbf{p}}(n)\|^2} \\ &= \frac{2|\tilde{\beta}|^2}{\sigma_\epsilon^2} \sum_{n=1}^L \|\tilde{\mathbf{p}}(n)\|^2. \end{aligned}$$

Given a detection threshold  $\gamma$  and  $\tilde{\beta} \neq 0$ , which means the target is present, the probability of detecting the target is

$$P_D(\theta|\tilde{\beta}) = p(|\check{y}|^2 > \gamma|\tilde{\beta}) = Q_1\left(\sqrt{\frac{2|\tilde{\beta}|^2}{\sigma_\epsilon^2} \sum_{n=1}^L \|\tilde{\mathbf{p}}(n)\|^2}, \sqrt{\gamma}\right),$$

where  $Q_1(\cdot, \cdot)$  is the Marcum Q-function. This function can be numerically approximated, which is useful for evaluating the detection probability in practical applications [17, p. 47].

In the opposite case,  $\tilde{\beta} = 0$ , which means the target is absent, and the non-centrality parameter  $\lambda = 0$ . The probability of a false alarm is given as

$$P_{FA} = p(|\check{y}|^2 > \gamma|\tilde{\beta} = 0) = Q_1(0, \sqrt{\gamma}) = e^{-\frac{\gamma}{2}}.$$

The last equation stems from the property of the Marcum Q-function  $Q_1(0, x) = e^{-\frac{x^2}{2}}$  [17, p. 48]. Thus, we isolate  $\gamma$  in the above equation, and we get  $\gamma = -2 \log p_{FA}$ .

### 3.3. Detection Probability

The Marcum Q-function computes the  $P_D$  of a specific value  $\tilde{\beta}$ . This can result in a random outcome. To solve this problem, we calculate the expectation over the distribution of  $\tilde{\beta}$ . The expected detection probability is

$$P_D(\theta) = \mathbb{E}_{\tilde{\beta}} \left\{ Q_1 \left( \sqrt{\frac{2|\tilde{\beta}|^2}{\sigma_{\epsilon}^2} \sum_{n=1}^L \|\tilde{\mathbf{p}}(n)\|^2}, \sqrt{\gamma} \right) \right\}.$$

The expected detection probability can be numerically calculated as the ensemble average with respect to  $\tilde{\beta}$ . This chapter concludes the communication and radar theory needed to design dual-functional waveforms.

## 4 Optimisation Methods

To design a dual-functional waveform with a trade-off between radar and communication, optimisation problems for different beampatterns must be derived and solved. Therefore, in this chapter, the two necessary optimisation problems will be reviewed. These two methods are the orthogonal Procrustes problem and the trust region subproblem (TRS).

### 4.1 Orthogonal Procrustes Problem

In the orthogonal Procrustes problem, one seeks to find a matrix with orthonormal rows  $\mathbf{Q}$  that minimises

$$\|\mathbf{A}\mathbf{Q} - \mathbf{B}\|_F^2,$$

where  $\|\cdot\|_F$  denotes the Frobenius norm.

#### Theorem 4.1 (Orthogonal Procrustes Problem)

Let  $\mathbf{A} \in \mathbb{C}^{m \times n}$ , and  $\mathbf{B} \in \mathbb{C}^{m \times a}$  be given, and  $\mathbf{Q} \in \mathbb{C}^{n \times a}$  with  $n \leq a$  be a unitary matrix when  $n = a$ . Then, the orthogonal Procrustes problem is given by

$$\begin{aligned} \min_{\mathbf{Q}} \quad & \|\mathbf{A}\mathbf{Q} - \mathbf{B}\|_F^2 \\ \text{s.t.} \quad & \mathbf{Q}\mathbf{Q}^H = \mathbf{I}_n, \end{aligned}$$

and have a global minimum at

$$\mathbf{Q}_{opt} = \mathbf{V}\mathbf{I}_{n \times a}\mathbf{U}^H,$$

where  $\mathbf{I}_{n \times a} = \begin{bmatrix} \mathbf{I}_n & \mathbf{0}_{n \times (a-n)} \end{bmatrix}$  and  $\mathbf{U}\mathbf{\Sigma}\mathbf{V}^H$  is the singular value decomposition (SVD) of  $\mathbf{B}^H\mathbf{A}$ . [23, Definition 1.0.2]

#### Proof

First, the objective function is rewritten using the Frobenius norm as defined in Definition A.4

$$\begin{aligned} \|\mathbf{A}\mathbf{Q} - \mathbf{B}\|_F^2 &= \text{Tr}\left((\mathbf{A}\mathbf{Q} - \mathbf{B})^H(\mathbf{A}\mathbf{Q} - \mathbf{B})\right) \\ &= \text{Tr}\left(\mathbf{Q}^H\mathbf{A}^H\mathbf{A}\mathbf{Q}\right) - \text{Tr}\left(\mathbf{B}^H\mathbf{A}\mathbf{Q}\right) - \text{Tr}\left(\mathbf{Q}^H\mathbf{A}^H\mathbf{B}\right) + \text{Tr}\left(\mathbf{B}^H\mathbf{B}\right). \end{aligned}$$

Using the cyclic property of trace Lemma A.2 and the fact that  $\text{Tr}(\mathbf{A}^H) = \overline{\text{Tr}(\mathbf{A})}$  by Lemma A.3

$$= \text{Tr}\left(\mathbf{Q}\mathbf{Q}^H\mathbf{A}^H\mathbf{A}\right) - \text{Tr}\left(\mathbf{Q}\mathbf{B}^H\mathbf{A}\right) - \overline{\text{Tr}\left(\mathbf{Q}\mathbf{B}^H\mathbf{A}\right)} + \text{Tr}\left(\mathbf{B}^H\mathbf{B}\right).$$

## 4.2. Trust Region Subproblem

Using that  $\mathbf{Q}\mathbf{Q}^H = \mathbf{I}_n$

$$\|\mathbf{A}\mathbf{Q} - \mathbf{B}\|_F^2 = \|\mathbf{A}\|_F^2 - 2\operatorname{Re}\left\{\operatorname{Tr}\left(\mathbf{Q}\mathbf{B}^H\mathbf{A}\right)\right\} + \|\mathbf{B}\|_F^2. \quad (4.1)$$

Hence, (4.1) can be minimised by maximising  $\operatorname{Re}\left\{\operatorname{Tr}\left(\mathbf{Q}\mathbf{B}^H\mathbf{A}\right)\right\}$ . Let  $\mathbf{U}\mathbf{\Sigma}\mathbf{V}^H$  be the SVD of  $\mathbf{B}^H\mathbf{A}$ , where  $\mathbf{U} \in \mathbb{C}^{a \times a}$ ,  $\mathbf{\Sigma} \in \mathbb{C}^{a \times n}$ , and  $\mathbf{V} \in \mathbb{C}^{n \times n}$ . Then we have

$$\begin{aligned} \operatorname{Re}\left\{\operatorname{Tr}\left(\mathbf{Q}\mathbf{B}^H\mathbf{A}\right)\right\} &= \operatorname{Re}\left\{\operatorname{Tr}\left(\mathbf{Q}\mathbf{U}\mathbf{\Sigma}\mathbf{V}^H\right)\right\} \\ &= \operatorname{Re}\left\{\operatorname{Tr}\left(\mathbf{\Sigma}\mathbf{V}^H\mathbf{Q}\mathbf{U}\right)\right\}, \end{aligned}$$

let  $\mathbf{Z} = \mathbf{V}^H\mathbf{Q}\mathbf{U}$

$$\begin{aligned} &= \operatorname{Re}\left\{\operatorname{Tr}(\mathbf{\Sigma}\mathbf{Z})\right\} \\ &= \operatorname{Re}\left\{\sum_{i=1}^d \sigma_{i,i} z_{i,i}\right\}, \end{aligned} \quad (4.2)$$

where  $d$  is the number of non-zero singular values and  $\sigma_{i,i}$  are the singular values of  $\mathbf{B}^H\mathbf{A}$ .  $\mathbf{Z} \in \mathbb{C}^{n \times a}$  has orthonormal rows because it is a product of matrices with orthonormal rows, and since  $\mathbf{\Sigma}$  is a diagonal matrix, (4.2) can be maximised by choosing  $\mathbf{Z} = \mathbf{I}_{n \times a}$ . From this,  $\mathbf{Q}_{opt}$  can be obtained as

$$\mathbf{I}_{n \times a} = \mathbf{V}^H \mathbf{Q}_{opt} \mathbf{U} \Leftrightarrow \mathbf{Q}_{opt} = \mathbf{V} \mathbf{I}_{n \times a} \mathbf{U}^H. \quad \blacksquare$$

To solve the second optimisation problem for a dual-functional waveform with a trade-off design between radar and communication, the trust region method is used.

## 4.2 Trust Region Subproblem

The idea behind trust region methods is to minimise the quadratic model at each iteration as in Newton's method, but we restrict ourselves to a ball-shaped region, called the trust region. At each iteration, the TRS must be solved. In the optimisation problem for a trade-off design we need to solve the TRS for complex-valued matrices rewritten as vectors. Therefore, the TRS will be defined for complex vectors in this project. The TRS is defined as

$$\begin{aligned} \min \quad & q(\mathbf{x}) = \mathbf{x}^H \mathbf{A} \mathbf{x} - 2\operatorname{Re}\left\{\mathbf{a}^H \mathbf{x}\right\} \\ \text{s.t.} \quad & \|\mathbf{x}\|_2^2 \leq s^2, \end{aligned} \quad (4.3)$$

where  $\mathbf{A} \in \mathbb{C}^{n \times n}$  is a Hermitian matrix,  $\mathbf{a} \in \mathbb{C}^n$  is known,  $\mathbf{x} \in \mathbb{C}^n$  is a vector of unknowns, and  $s$  is a positive scalar [5, p. 1]. The first term of the objective function is always real, as shown in Lemma A.5.

The Karush-Kuhn-Tucker (KKT) necessary conditions for the TRS are established in the



#### 4.2. Trust Region Subproblem

following theorem. Any optimal point to an optimisation problem with a differentiable objective and constraint function must satisfy the KKT conditions [3, p. 243].

##### Theorem 4.2 (Necessary and Sufficient Conditions)

The point  $\mathbf{x}_{opt}$  is a solution to the trust region subproblem if and only if

$$\begin{aligned}\|\mathbf{x}_{opt}\|_2^2 &\leq s^2, \\ (\mathbf{A} - \lambda_{opt}\mathbf{I}_n)\mathbf{x}_{opt} &= \mathbf{a}, \\ \lambda_{opt}(\|\mathbf{x}_{opt}\|_2^2 - s^2) &= 0, \\ \mathbf{A} - \lambda_{opt}\mathbf{I}_n &\succeq 0, \\ \lambda_{opt} &\leq 0,\end{aligned}$$

where  $\lambda_{opt}$  is a Lagrange multiplier and  $\succeq$  denotes that  $\mathbf{A} - \lambda_{opt}\mathbf{I}_n$  is positive semidefinite. [5, Theorem 3.1]

##### Proof

"  $\Rightarrow$  " : First, we will prove that if  $\mathbf{x}_{opt}$  is a solution to the TRS, then the second order necessary condition can be strengthened to  $\mathbf{A} - \lambda_{opt}\mathbf{I}_n \succeq 0$ . Suppose that  $\mathbf{x}_{opt}$  is a solution to the TRS in (4.3). We can assume that the trivial case  $\mathbf{x}_{opt} = \mathbf{0}$  does not hold since  $s > 0$ . The lagrangian function is

$$\mathcal{L}(\mathbf{x}, \lambda) = \mathbf{x}^H \mathbf{A} \mathbf{x} - 2\text{Re} \left\{ \mathbf{a}^H \mathbf{x} \right\} - \lambda (\|\mathbf{x}\|^2 - s^2).$$

The KKT conditions for the TRS yield

- $\|\mathbf{x}_{opt}\|_2^2 \leq s^2$  (Feasibility),
- $\nabla_{\mathbf{x}} \mathcal{L}(\mathbf{x}_{opt}, \lambda_{opt}) = (\mathbf{A} - \lambda_{opt}\mathbf{I}_n)\mathbf{x}_{opt} - \mathbf{a} = \mathbf{0}$  (Stationarity),
- $\lambda_{opt}(\|\mathbf{x}_{opt}\|_2^2 - s^2) = 0$  (Complementary Slackness),
- $\lambda_{opt} \leq 0$ ,
- and if  $\|\mathbf{x}_{opt}\|_2^2 = s^2$ ,  $0 \leq \mathbf{y}^H (\mathbf{A} - \lambda_{opt}\mathbf{I}_n) \mathbf{y}$  for all  $\mathbf{y}$  such that  $\mathbf{y}^H \mathbf{x}_{opt} = 0$  (2nd order necessary condition).

Since  $\mathbf{x}_{opt}$  solves the TRS, the following inequality must hold true for the objective function  $q(\mathbf{x}_{opt}) \leq q(\mathbf{x})$  for all  $\mathbf{x}$  satisfying  $\|\mathbf{x}\|_2^2 = \|\mathbf{x}_{opt}\|_2^2$ . Combined with  $(\mathbf{A} - \lambda_{opt}\mathbf{I}_n)\mathbf{x}_{opt} = \mathbf{a}$  this yields

$$\begin{aligned}\mathbf{x}_{opt}^H \mathbf{A} \mathbf{x}_{opt} - 2\text{Re} \left\{ \mathbf{x}_{opt}^H (\mathbf{A} - \lambda_{opt}\mathbf{I}_n) \mathbf{x}_{opt} \right\} &\leq \mathbf{x}^H \mathbf{A} \mathbf{x} - 2\text{Re} \left\{ \mathbf{x}_{opt}^H (\mathbf{A} - \lambda_{opt}\mathbf{I}_n) \mathbf{x} \right\} \\ -\mathbf{x}^H \mathbf{A} \mathbf{x} + 2\text{Re} \left\{ \mathbf{x}_{opt}^H (\mathbf{A} - \lambda_{opt}\mathbf{I}_n) \mathbf{x} \right\} &\leq -\mathbf{x}_{opt}^H \mathbf{A} \mathbf{x}_{opt} + 2\text{Re} \left\{ \mathbf{x}_{opt}^H (\mathbf{A} - \lambda_{opt}\mathbf{I}_n) \mathbf{x}_{opt} \right\} \\ &= -\mathbf{x}_{opt}^H \mathbf{A} \mathbf{x}_{opt} + 2\text{Re} \left\{ \mathbf{x}_{opt}^H \mathbf{A} \mathbf{x}_{opt} - \mathbf{x}_{opt}^H \lambda_{opt} \mathbf{I}_n \mathbf{x}_{opt} \right\}\end{aligned}$$

#### 4.2. Trust Region Subproblem

By Lemma A.5 we can write

$$\begin{aligned} -\mathbf{x}^H \mathbf{A} \mathbf{x} + 2 \operatorname{Re} \left\{ \mathbf{x}_{opt}^H (\mathbf{A} - \lambda_{opt} \mathbf{I}_n) \mathbf{x} \right\} &\leq -\mathbf{x}_{opt}^H \mathbf{A} \mathbf{x}_{opt} + 2 \mathbf{x}_{opt}^H \mathbf{A} \mathbf{x}_{opt} - 2 \mathbf{x}_{opt}^H \lambda_{opt} \mathbf{I}_n \mathbf{x}_{opt} \\ &= \mathbf{x}_{opt}^H \mathbf{A} \mathbf{x}_{opt} - 2 \mathbf{x}_{opt}^H \lambda_{opt} \mathbf{I}_n \mathbf{x}_{opt} \end{aligned}$$

Using that  $\mathbf{x}_{opt}^H \mathbf{x}_{opt} = \|\mathbf{x}_{opt}\|_2^2 = \|\mathbf{x}\|_2^2 = \mathbf{x}^H \mathbf{x}$  we can write

$$\begin{aligned} 0 &\leq \mathbf{x}_{opt}^H \mathbf{A} \mathbf{x}_{opt} - \mathbf{x}_{opt}^H \lambda_{opt} \mathbf{I}_n \mathbf{x}_{opt} + \mathbf{x}^H \mathbf{A} \mathbf{x} - \mathbf{x}^H \lambda_{opt} \mathbf{I}_n \mathbf{x} - 2 \operatorname{Re} \left\{ \mathbf{x}_{opt}^H (\mathbf{A} - \lambda_{opt} \mathbf{I}_n) \mathbf{x} \right\} \\ &= \mathbf{x}_{opt}^H (\mathbf{A} - \lambda_{opt} \mathbf{I}_n) \mathbf{x}_{opt} + \mathbf{x}^H (\mathbf{A} - \lambda_{opt} \mathbf{I}_n) \mathbf{x} - 2 \operatorname{Re} \left\{ \mathbf{x}_{opt}^H (\mathbf{A} - \lambda_{opt} \mathbf{I}_n) \mathbf{x} \right\} \\ &= \mathbf{x}_{opt}^H (\mathbf{A} - \lambda_{opt} \mathbf{I}_n) \mathbf{x}_{opt} + \mathbf{x}^H (\mathbf{A} - \lambda_{opt} \mathbf{I}_n) \mathbf{x} - \mathbf{x}_{opt}^H (\mathbf{A} - \lambda_{opt} \mathbf{I}_n) \mathbf{x} - \overline{\mathbf{x}_{opt}^H (\mathbf{A} - \lambda_{opt} \mathbf{I}_n) \mathbf{x}} \\ &= \mathbf{x}_{opt}^H (\mathbf{A} - \lambda_{opt} \mathbf{I}_n) \mathbf{x}_{opt} + \mathbf{x}^H (\mathbf{A} - \lambda_{opt} \mathbf{I}_n) \mathbf{x} - \mathbf{x}_{opt}^H (\mathbf{A} - \lambda_{opt} \mathbf{I}_n) \mathbf{x} - \mathbf{x}^H (\mathbf{A} - \lambda_{opt} \mathbf{I}_n) \mathbf{x}_{opt} \\ &= (\mathbf{x}_{opt}^H (\mathbf{A} - \lambda_{opt} \mathbf{I}_n) - \mathbf{x}^H (\mathbf{A} - \lambda_{opt} \mathbf{I}_n)) (\mathbf{x}_{opt} - \mathbf{x}) \\ &= (\mathbf{x}_{opt} - \mathbf{x})^H (\mathbf{A} - \lambda_{opt} \mathbf{I}_n) (\mathbf{x}_{opt} - \mathbf{x}). \end{aligned}$$

This can be rewritten as

$$0 \leq \mathbf{y}^H (\mathbf{A} - \lambda_{opt} \mathbf{I}_n) \mathbf{y} \quad \text{for all } \mathbf{y} \text{ such that } \mathbf{y}^H \mathbf{x}_{opt} \neq 0, \quad (4.4)$$

where  $\mathbf{y} = \alpha (\mathbf{x}_{opt} - \mathbf{x})$  for a well chosen  $\alpha \neq 0$  and  $\mathbf{x}$ . Let  $\alpha = \frac{\|\mathbf{y}\|_2^2}{2 \mathbf{y}^H \mathbf{x}_{opt}}$  and  $\mathbf{x} = \mathbf{x}_{opt} - \frac{1}{\alpha} \mathbf{y}$ . Then (4.4) in addition to the second order necessary condition yields

$$\mathbf{A} - \lambda_{opt} \mathbf{I}_n \succeq 0.$$

"  $\Leftarrow$  " : Next we will prove that if the necessary and sufficient conditions are fulfilled, then  $\mathbf{x}_{opt}$  is a solution to the TRS. Let  $\mathbf{x}_{opt}$  and  $\lambda_{opt} \leq 0$  be a solution to the following equations

$$\begin{aligned} \|\mathbf{x}_{opt}\|_2^2 &\leq s^2, \\ (\mathbf{A} - \lambda_{opt} \mathbf{I}_n) \mathbf{x}_{opt} &= \mathbf{a}, \\ \lambda_{opt} (\|\mathbf{x}_{opt}\|_2^2 - s^2) &= 0, \\ \mathbf{A} - \lambda_{opt} \mathbf{I}_n &\succeq 0. \end{aligned}$$

Then, for any  $\mathbf{x} \in \mathbb{C}^n$

$$\begin{aligned} 0 &\leq (\mathbf{x}_{opt} - \mathbf{x})^H (\mathbf{A} - \lambda_{opt} \mathbf{I}_n) (\mathbf{x}_{opt} - \mathbf{x}) \\ &= (\mathbf{x}_{opt}^H (\mathbf{A} - \lambda_{opt} \mathbf{I}_n) - \mathbf{x}^H (\mathbf{A} - \lambda_{opt} \mathbf{I}_n)) (\mathbf{x}_{opt} - \mathbf{x}) \\ &= \mathbf{x}_{opt}^H (\mathbf{A} - \lambda_{opt} \mathbf{I}_n) \mathbf{x}_{opt} + \mathbf{x}^H (\mathbf{A} - \lambda_{opt} \mathbf{I}_n) \mathbf{x} - \mathbf{x}_{opt}^H (\mathbf{A} - \lambda_{opt} \mathbf{I}_n) \mathbf{x} - \overline{\mathbf{x}_{opt}^H (\mathbf{A} - \lambda_{opt} \mathbf{I}_n) \mathbf{x}} \\ &= \mathbf{x}_{opt}^H (\mathbf{A} - \lambda_{opt} \mathbf{I}_n) \mathbf{x}_{opt} + \mathbf{x}^H (\mathbf{A} - \lambda_{opt} \mathbf{I}_n) \mathbf{x} - \mathbf{x}_{opt}^H (\mathbf{A} - \lambda_{opt} \mathbf{I}_n) \mathbf{x} - \mathbf{x}^H (\mathbf{A} - \lambda_{opt} \mathbf{I}_n) \mathbf{x}_{opt} \\ &= \mathbf{x}_{opt}^H (\mathbf{A} - \lambda_{opt} \mathbf{I}_n) \mathbf{x}_{opt} + \mathbf{x}^H (\mathbf{A} - \lambda_{opt} \mathbf{I}_n) \mathbf{x} - 2 \operatorname{Re} \left\{ \mathbf{x}_{opt}^H (\mathbf{A} - \lambda_{opt} \mathbf{I}_n) \mathbf{x} \right\} \\ &= -\mathbf{x}_{opt}^H (\mathbf{A} - \lambda_{opt} \mathbf{I}_n) \mathbf{x}_{opt} + 2 \mathbf{x}_{opt}^H (\mathbf{A} - \lambda_{opt} \mathbf{I}_n) \mathbf{x}_{opt} \\ &\quad + \mathbf{x}^H (\mathbf{A} - \lambda_{opt} \mathbf{I}_n) \mathbf{x} - 2 \operatorname{Re} \left\{ \mathbf{x}_{opt}^H (\mathbf{A} - \lambda_{opt} \mathbf{I}_n) \mathbf{x} \right\}. \end{aligned}$$

#### 4.2. Trust Region Subproblem

By Lemma A.5, this can be rewritten as

$$0 \leq -\mathbf{x}_{opt}^H (\mathbf{A} - \lambda_{opt} \mathbf{I}_n) \mathbf{x}_{opt} + 2 \operatorname{Re} \left\{ \mathbf{x}_{opt}^H (\mathbf{A} - \lambda_{opt} \mathbf{I}_n) \mathbf{x}_{opt} \right\} \\ + \mathbf{x}^H (\mathbf{A} - \lambda_{opt} \mathbf{I}_n) \mathbf{x} - 2 \operatorname{Re} \left\{ \mathbf{x}_{opt}^H (\mathbf{A} - \lambda_{opt} \mathbf{I}_n) \mathbf{x} \right\}.$$

Recall that  $(\mathbf{A} - \lambda_{opt} \mathbf{I}_n) \mathbf{x}_{opt} = \mathbf{a}$

$$0 \leq -\mathbf{x}_{opt}^H (\mathbf{A} - \lambda_{opt} \mathbf{I}_n) \mathbf{x}_{opt} + 2 \operatorname{Re} \left\{ \mathbf{a}^H \mathbf{x}_{opt} \right\} + \mathbf{x}^H (\mathbf{A} - \lambda_{opt} \mathbf{I}_n) \mathbf{x} - 2 \operatorname{Re} \left\{ \mathbf{a}^H \mathbf{x} \right\} \\ = -\mathbf{x}_{opt}^H \mathbf{A} \mathbf{x}_{opt} + \mathbf{x}_{opt}^H \lambda_{opt} \mathbf{I}_n \mathbf{x}_{opt} + 2 \operatorname{Re} \left\{ \mathbf{a}^H \mathbf{x}_{opt} \right\} + \mathbf{x}^H \mathbf{A} \mathbf{x} - \mathbf{x}^H \lambda_{opt} \mathbf{I}_n \mathbf{x} - 2 \operatorname{Re} \left\{ \mathbf{a}^H \mathbf{x} \right\} \quad (4.5)$$

The objective functions  $q(\mathbf{x})$  and  $q(\mathbf{x}_{opt})$  appear in (4.5). This yields

$$0 \leq -q(\mathbf{x}_{opt}) + \mathbf{x}_{opt}^H \lambda_{opt} \mathbf{I}_n \mathbf{x}_{opt} + q(\mathbf{x}) - \mathbf{x}^H \lambda_{opt} \mathbf{I}_n \mathbf{x}.$$

We can now formulate

$$q(\mathbf{x}_{opt}) - \mathbf{x}_{opt}^H \lambda_{opt} \mathbf{I}_n \mathbf{x}_{opt} + \mathbf{x}^H \lambda_{opt} \mathbf{I}_n \mathbf{x} \leq q(\mathbf{x}) \\ q(\mathbf{x}_{opt}) - \lambda_{opt} (\|\mathbf{x}_{opt}\|_2^2 - \|\mathbf{x}\|_2^2) \leq q(\mathbf{x}). \quad (4.6)$$

Since  $\lambda_{opt} (\|\mathbf{x}_{opt}\|_2^2 - s^2) = 0$ , either  $\lambda_{opt} = 0$  or  $\|\mathbf{x}_{opt}\|_2^2 = s^2$ . If  $\lambda_{opt} = 0$  then (4.6) implies that  $\mathbf{x}_{opt}$  is a solution to the TRS. If  $\|\mathbf{x}_{opt}\|_2^2 = s^2$  then for all  $\mathbf{x}$  such that  $\|\mathbf{x}\|_2^2 \leq s^2$  it holds that  $-\lambda_{opt} (\|\mathbf{x}_{opt}\|_2^2 - s^2) \geq 0$  and again (4.6) implies that  $\mathbf{x}_{opt}$  is a solution to the TRS. ■

Having presented the necessary optimisation methods, some waveform designs will be derived in the next chapter.

## 5 Waveform Design

In this chapter, the orthogonal Proscutes problem and TRS optimisation methods as presented in Chapter 4 will be used to design the dual-functional waveforms. The waveforms will be designed for an omnidirectional and directional beampattern. Furthermore, a trade-off design with a total power constraint will be derived.

### 5.1 Omnidirectional Beampattern Design with a Strict Equality Constraint

In this section, the beampattern design is considered to be omnidirectional. Therefore, the columns of the transmitted waveform  $\mathbf{X}$  must be orthogonal such that each antenna's signal is uncorrelated to each other.

As stated in Section 2.3, a minimal SEP can be achieved by minimising the MUI energy. Thereby, for a waveform with an omnidirectional beampattern the SEP can be minimised by solving the minimisation problem

$$\begin{aligned} \min_{\mathbf{X}} \quad & \|\mathbf{H}\mathbf{X} - \mathbf{S}\|_F^2 \\ \text{s.t.} \quad & \frac{1}{L}\mathbf{X}\mathbf{X}^H = \frac{P_T}{N}\mathbf{I}_N, \end{aligned} \quad (5.1)$$

[13, p. 4267]. The minimisation problem can be rewritten as an orthogonal Procrustes problem, as stated in Theorem 4.1. This is achieved by making the substitution

$$\tilde{\mathbf{X}} = \sqrt{\frac{N}{LP_T}}\mathbf{X} \iff \mathbf{X} = \sqrt{\frac{LP_T}{N}}\tilde{\mathbf{X}}. \quad (5.2)$$

We obtain a minimisation problem for  $\tilde{\mathbf{X}}$

$$\begin{aligned} \min_{\tilde{\mathbf{X}}} \quad & \left\| \sqrt{\frac{LP_T}{N}}\mathbf{H}\tilde{\mathbf{X}} - \mathbf{S} \right\|_F^2 \\ \text{s.t.} \quad & \tilde{\mathbf{X}}\tilde{\mathbf{X}}^H = \mathbf{I}_N. \end{aligned} \quad (5.3)$$

In the proof of Theorem 4.1 it was shown that the minimisation problem is equivalent to maximising

$$\sqrt{\frac{LP_T}{N}} \operatorname{Re}\left\{ \operatorname{Tr}\left(\tilde{\mathbf{X}}\mathbf{S}^H\mathbf{H}\right) \right\}, \quad (5.4)$$

thereby the scalar  $\sqrt{\frac{LP_T}{N}}$  can be disregarded in (5.3). The minimisation problem with  $\tilde{\mathbf{X}}$  can be solved by following the proof of Theorem 4.1. Let  $\mathbf{V}\Sigma\mathbf{U}^H$  be the SVD of  $\mathbf{S}^H\mathbf{H}$ , then the solution to (5.3) is

$$\tilde{\mathbf{X}} = \mathbf{V}\mathbf{I}_{N \times L}\mathbf{U}^H,$$

## 5.2. Directional Beampattern Design with a Strict Equality Constraint

where  $\mathbf{U} \in \mathbb{C}^{N \times N}$  and  $\mathbf{V} \in \mathbb{C}^{L \times L}$  are both unitary matrices, and  $\mathbf{I}_{N \times L} = \begin{bmatrix} \mathbf{I}_N & \mathbf{0}_{N \times (L-N)} \end{bmatrix}$ . Lastly, we can find the solution for the original minimisation problem (5.1) by substituting  $\tilde{\mathbf{X}}$  into (5.2) which yields

$$\mathbf{x}_{opt} = \sqrt{\frac{LP_T}{N}} \mathbf{V} \mathbf{I}_{N \times L} \mathbf{U}^H.$$

## 5.2 Directional Beampattern Design with a Strict Equality Constraint

In this section, the beampattern design is considered to be directional.  $\mathbf{R}$  is assumed to be given and is designed such that the waveform has a per-antenna power constraint. The waveform can be found by solving the MUI minimisation problem

$$\begin{aligned} \min_{\mathbf{X}} \quad & \|\mathbf{H}\mathbf{X} - \mathbf{S}\|_F^2 \\ \text{s.t.} \quad & \frac{1}{L} \mathbf{X}\mathbf{X}^H = \mathbf{R}, \end{aligned} \quad (5.5)$$

where  $\mathbf{R}$  is the covariance matrix defined as (3.3) and is assumed to be a Hermitian positive definite matrix [13, p. 4267]. Hence,  $\mathbf{R}$  can be Cholesky decomposed

$$\mathbf{R} = \mathbf{F}\mathbf{F}^H,$$

where  $\mathbf{F} \in \mathbb{C}^{N \times N}$  is a lower triangular invertible matrix [11, Theorem 18.26]. The equality constraint can be reformulated as

$$\frac{1}{L} \mathbf{F}^{-1} \mathbf{X}\mathbf{X}^H (\mathbf{F}^H)^{-1} = \mathbf{I}_N.$$

Then, the minimisation problem can be rewritten as an orthogonal Procrustes problem by making the substitution

$$\tilde{\mathbf{X}} = \sqrt{\frac{1}{L}} \mathbf{F}^{-1} \mathbf{X} \iff \mathbf{X} = \sqrt{L} \mathbf{F} \tilde{\mathbf{X}}. \quad (5.6)$$

Hence, the minimisation problem becomes

$$\begin{aligned} \min_{\tilde{\mathbf{X}}} \quad & \left\| \sqrt{L} \mathbf{H} \mathbf{F} \tilde{\mathbf{X}} - \mathbf{S} \right\|_F^2 \\ \text{s.t.} \quad & \tilde{\mathbf{X}} \tilde{\mathbf{X}}^H = \mathbf{I}_N. \end{aligned} \quad (5.7)$$

The scalar  $\sqrt{L}$  can again be disregarded by the same argument as in (5.4). The minimisation problem can be solved by following the proof of Theorem 4.1. Let  $\tilde{\mathbf{V}} \tilde{\Sigma} \tilde{\mathbf{U}}^H$  be the SVD of  $\mathbf{S}^H \mathbf{H} \mathbf{F}$ , then the solution to (5.7) is

$$\tilde{\mathbf{X}} = \tilde{\mathbf{V}} \mathbf{I}_{N \times L} \tilde{\mathbf{U}}^H.$$

The solution to the original optimisation problem (5.5) can be found by substituting  $\tilde{\mathbf{X}}$  into (5.6), hence

$$\mathbf{x}_{opt} = \sqrt{L} \mathbf{F} \tilde{\mathbf{V}} \mathbf{I}_{N \times L} \tilde{\mathbf{U}}^H.$$

### 5.3 Trade-off Design with a Total Power Constraint

In this section, a waveform design with a trade-off between radar and communication performance is considered. The waveform is designed with a total power constraint. Let  $\mathbf{X}_0$  be a waveform with a desirable radar beampattern, for instance, the waveform derived in Section 5.1 or Section 5.2. Then the minimisation problem for trade-off design with a total power constraint is given as

$$\begin{aligned} \min_{\mathbf{X}} \quad & \rho \|\mathbf{H}\mathbf{X} - \mathbf{S}\|_F^2 + (1 - \rho) \|\mathbf{X} - \mathbf{X}_0\|_F^2 \\ \text{s.t.} \quad & \frac{1}{L} \|\mathbf{X}\|_F^2 \leq P_T, \end{aligned} \quad (5.8)$$

where  $0 \leq \rho \leq 1$  is a weighting factor for radar and communication performance [13, p. 4268]. If  $\rho = 0$ , the radar is given full priority, and if  $\rho = 1$ , the communication is given full priority. The minimisation problem shows a total power constraint as an inequality. However, in this project, we intend to find a solution on the boundary of this constraint, aiming for the optimal solution that fully utilises the allowed power budget.

In order to obtain a solution to (5.8), the objective function is rewritten [13, p. 4268].

$$\begin{aligned} \rho \|\mathbf{H}\mathbf{X} - \mathbf{S}\|_F^2 + (1 - \rho) \|\mathbf{X} - \mathbf{X}_0\|_F^2 &= \|\sqrt{\rho}\mathbf{H}\mathbf{X} - \sqrt{\rho}\mathbf{S}\|_F^2 + \|\sqrt{1 - \rho}\mathbf{X} - \sqrt{1 - \rho}\mathbf{X}_0\|_F^2 \\ &= \left\| \begin{bmatrix} \sqrt{\rho}\mathbf{H} \\ \sqrt{1 - \rho}\mathbf{I}_N \end{bmatrix} \mathbf{X} - \begin{bmatrix} \sqrt{\rho}\mathbf{S} \\ \sqrt{1 - \rho}\mathbf{X}_0 \end{bmatrix} \right\|_F^2 \\ &= \left\| \begin{bmatrix} \sqrt{\rho}\mathbf{H}^T & \sqrt{1 - \rho}\mathbf{I}_N \end{bmatrix}^T \mathbf{X} - \begin{bmatrix} \sqrt{\rho}\mathbf{S}^T & \sqrt{1 - \rho}\mathbf{X}_0^T \end{bmatrix}^T \right\|_F^2. \end{aligned}$$

Denote

$$\mathbf{A} = \begin{bmatrix} \sqrt{\rho}\mathbf{H}^T & \sqrt{1 - \rho}\mathbf{I}_N \end{bmatrix}^T \quad \text{and} \quad \mathbf{B} = \begin{bmatrix} \sqrt{\rho}\mathbf{S}^T & \sqrt{1 - \rho}\mathbf{X}_0^T \end{bmatrix}^T,$$

where  $\mathbf{A} \in \mathbb{C}^{(K+N) \times N}$  and  $\mathbf{B} \in \mathbb{C}^{(K+N) \times L}$ . Then, the minimisation problem is given as

$$\begin{aligned} \min_{\mathbf{X}} \quad & \|\mathbf{A}\mathbf{X} - \mathbf{B}\|_F^2 \\ \text{s.t.} \quad & \|\mathbf{X}\|_F^2 \leq LP_T. \end{aligned} \quad (5.9)$$

The objective function (5.9) can once again be rewritten as

$$\begin{aligned} \|\mathbf{A}\mathbf{X} - \mathbf{B}\|_F^2 &= \text{Tr} \left( (\mathbf{A}\mathbf{X} - \mathbf{B})^H (\mathbf{A}\mathbf{X} - \mathbf{B}) \right) \\ &= \text{Tr} \left( \mathbf{X}^H \mathbf{A}^H \mathbf{A} \mathbf{X} \right) - \text{Tr} \left( \mathbf{X}^H \mathbf{A}^H \mathbf{B} \right) - \text{Tr} \left( \mathbf{B}^H \mathbf{A} \mathbf{X} \right) + \text{Tr} \left( \mathbf{B}^H \mathbf{B} \right). \end{aligned} \quad (5.10)$$

Define

$$\mathbf{Q} = \mathbf{A}^H \mathbf{A} \in \mathbb{C}^{N \times N} \quad \text{and} \quad \mathbf{G} = \mathbf{A}^H \mathbf{B} \in \mathbb{C}^{N \times L}.$$

By the cyclic property of trace Lemma A.2 and Lemma A.3, the expression in (5.10) can be written as

$$\begin{aligned} & \text{Tr} \left( \mathbf{X}^H \mathbf{Q} \mathbf{X} \right) - \text{Tr} \left( \mathbf{X}^H \mathbf{G} \right) - \text{Tr} \left( \mathbf{G}^H \mathbf{X} \right) + \text{Tr} \left( \mathbf{B}^H \mathbf{B} \right) \\ &= \text{Tr} \left( \mathbf{X}^H \mathbf{Q} \mathbf{X} \right) - \overline{\text{Tr} \left( \mathbf{G}^H \mathbf{X} \right)} - \text{Tr} \left( \mathbf{G}^H \mathbf{X} \right) + \text{Tr} \left( \mathbf{B}^H \mathbf{B} \right) \\ &= \text{Tr} \left( \mathbf{X}^H \mathbf{Q} \mathbf{X} \right) - 2\text{Re} \left\{ \text{Tr} \left( \mathbf{G}^H \mathbf{X} \right) \right\} + \|\mathbf{B}\|_F^2, \end{aligned}$$

### 5.3. Trade-off Design with a Total Power Constraint

where  $\|\mathbf{B}\|_F^2$  is disregarded in the minimisation problem since it does not depend on  $\mathbf{X}$ . Then, the minimisation problem is given as

$$\begin{aligned} \min_{\mathbf{X}} \quad & \text{Tr}(\mathbf{X}^H \mathbf{Q} \mathbf{X}) - 2\text{Re} \left\{ \text{Tr}(\mathbf{G}^H \mathbf{X}) \right\} \\ \text{s.t.} \quad & \|\mathbf{X}\|_F^2 \leq LP_T. \end{aligned} \quad (5.11)$$

It is clear from the definition of  $\mathbf{Q}$  that it is a Hermitian matrix. In order to find a solution to the minimisation problem, it should be reformulated as a vector minimisation problem. Let  $\mathbf{x}_i$  and  $\mathbf{g}_i$  denote the  $i$ 'th column vector of  $\mathbf{X}$  and  $\mathbf{G}$ , respectively. Then, the following vectors can be defined

$$\tilde{\mathbf{x}} = \begin{bmatrix} \mathbf{x}_1 \\ \mathbf{x}_2 \\ \mathbf{x}_3 \\ \vdots \\ \mathbf{x}_L \end{bmatrix} \in \mathbb{C}^{NL}, \quad \tilde{\mathbf{g}} = \begin{bmatrix} \mathbf{g}_1 \\ \mathbf{g}_2 \\ \mathbf{g}_3 \\ \vdots \\ \mathbf{g}_L \end{bmatrix} \in \mathbb{C}^{NL}.$$

We define a matrix  $\tilde{\mathbf{Q}}$  as

$$\tilde{\mathbf{Q}} = \begin{bmatrix} \mathbf{Q} & \mathbf{0}_{N \times N} & \cdots & \mathbf{0}_{N \times N} \\ \mathbf{0}_{N \times N} & \mathbf{Q} & \cdots & \mathbf{0}_{N \times N} \\ \vdots & \vdots & \ddots & \vdots \\ \mathbf{0}_{N \times N} & \mathbf{0}_{N \times N} & \cdots & \mathbf{Q} \end{bmatrix} \in \mathbb{C}^{NL \times NL}$$

where  $\mathbf{0}_{N \times N}$  is a  $N \times N$  zero matrix. By using the above notation, the minimisation problem (5.11) can be written as

$$\begin{aligned} \min_{\tilde{\mathbf{x}}} \quad & \tilde{\mathbf{x}}^H \tilde{\mathbf{Q}} \tilde{\mathbf{x}} - 2\text{Re} \left\{ \tilde{\mathbf{g}}^H \tilde{\mathbf{x}} \right\} \\ \text{s.t.} \quad & \|\tilde{\mathbf{x}}\|_2^2 \leq LP_T. \end{aligned}$$

Note that since  $\mathbf{Q}$  is Hermitian, so is  $\tilde{\mathbf{Q}}$ . The optimisation problem is recognised as a complex TRS. Therefore, in the following, the KKT conditions for the optimisation problem will be stated. Let  $\tilde{\mathbf{x}}_{opt}$  and  $\lambda_{opt}$  be the optimal points. Then, by Theorem 4.2 the following holds

$$\|\tilde{\mathbf{x}}_{opt}\|_2^2 \leq LP_T,$$

$$(\tilde{\mathbf{Q}} - \lambda_{opt} \mathbf{I}_{NL}) \tilde{\mathbf{x}}_{opt} = \tilde{\mathbf{g}}, \quad (5.12)$$

$$\lambda_{opt} (\|\tilde{\mathbf{x}}_{opt}\|_2^2 - LP_T) = 0, \quad (5.13)$$

$$\tilde{\mathbf{Q}} - \lambda_{opt} \mathbf{I}_{NL} \succeq 0, \quad (5.14)$$

$$\lambda_{opt} \leq 0. \quad (5.15)$$

Note that (5.14) implies that  $\lambda_{opt} \leq \lambda_{min}$ , where  $\lambda_{min}$  is the smallest eigenvalue of  $\tilde{\mathbf{Q}}$ . When  $\lambda_{opt} < \lambda_{min}$  it is called the easy case and when  $\lambda_{opt} = \lambda_{min}$  it is called the hard case. In order to determine when we are in which case, the smallest eigenvalue of  $\tilde{\mathbf{Q}}$  can be calculated.

### 5.3. Trade-off Design with a Total Power Constraint

It is first noted that if  $\lambda$  is an eigenvalue of  $\mathbf{Q}$  then it is also an eigenvalue of  $\tilde{\mathbf{Q}}$  with multiplicity  $L$ . Hence, the smallest eigenvalue of  $\tilde{\mathbf{Q}}$  can be obtained by finding the smallest eigenvalue of  $\mathbf{Q}$ .  $\mathbf{Q}$  can be calculated as

$$\begin{aligned}\mathbf{Q} &= \mathbf{A}^H \mathbf{A} \\ &= \begin{bmatrix} \sqrt{\rho} \mathbf{H}^H & \sqrt{1-\rho} \mathbf{I}_N \end{bmatrix} \begin{bmatrix} \sqrt{\rho} \mathbf{H} \\ \sqrt{1-\rho} \mathbf{I}_N \end{bmatrix} \\ &= \rho \mathbf{H}^H \mathbf{H} + (1-\rho) \mathbf{I}_N.\end{aligned}$$

It is assumed that the channel is Rayleigh fading, hence, it can be assumed that  $\mathbf{H}$  has full rank. Furthermore, the rank of  $\mathbf{H}$  equals the rank of  $\mathbf{H}^H \mathbf{H}$ , i.e.,  $\text{rank}(\mathbf{H}) = \text{rank}(\mathbf{H}^H \mathbf{H}) = K$ . Then by the rank-nullity theorem [11, Theorem 10.9] it must hold that

$$\text{nullity}(\mathbf{H}^H \mathbf{H}) = N - K > 0,$$

where the inequality stems from the assumption that there are more antennas than users  $K < N$ . Since the nullity of  $\mathbf{H}^H \mathbf{H}$  is non-zero, there is at least one eigenvalue equal to zero.  $\mathbf{H}^H \mathbf{H}$  is a positive semi-definite matrix, hence, its eigenvalues are non-negative [11, Theorem 18.26]. It can be seen that the eigenvalues of  $\mathbf{Q}$  are the eigenvalues of  $\mathbf{H}^H \mathbf{H}$  plus  $1 - \rho$ . Therefore, the smallest eigenvalue of  $\mathbf{Q}$  and  $\tilde{\mathbf{Q}}$  is  $1 - \rho$ .

Using (5.15), it can be seen that

$$\lambda_{opt} \leq 0 \leq \lambda_{min} = 1 - \rho.$$

If  $0 \leq \rho < 1$ , we are always in the easy case, i.e.,  $\lambda_{opt} < \lambda_{min}$ . However, if  $\rho = 1$ , it is possible that we are in the hard case, i.e.,  $\lambda_{opt} = \lambda_{min}$ . Therefore, we first let  $0 \leq \rho < 1$  and examine the easy case.

#### The Easy Case

Based on (5.12), when isolating for  $\tilde{\mathbf{x}}_{opt}$ , the following function is defined

$$h(\lambda) = \begin{cases} (\tilde{\mathbf{Q}} - \lambda \mathbf{I}_{NL})^{-1} \tilde{\mathbf{g}} & \text{if } \lambda < \lambda_{min} \\ (\tilde{\mathbf{Q}} - \lambda \mathbf{I}_{NL})^{\dagger} \tilde{\mathbf{g}} & \text{if } \lambda = \lambda_{min} \end{cases}$$

where  $(\cdot)^{\dagger}$  denotes the Moore-Penrose pseudo-inverse. The function  $h(\lambda)$  is well defined when  $\lambda < \lambda_{min}$  since this implies that all the eigenvalues of  $\tilde{\mathbf{Q}} - \lambda \mathbf{I}_{NL}$  are non-zero, hence,  $\tilde{\mathbf{Q}} - \lambda \mathbf{I}_{NL}$  is invertible. If  $\lambda = \lambda_{min}$ , then  $\tilde{\mathbf{Q}} - \lambda \mathbf{I}_{NL}$  is not invertible, and so the Moore-Penrose pseudo-inverse is used [28, p. 4]. The Moore-Penrose pseudo-inverse equals the standard inverse when  $\tilde{\mathbf{Q}} - \lambda_{opt} \mathbf{I}_{NL}$  is invertible. Therefore, it follows that

$$h(\lambda_{opt}) = (\tilde{\mathbf{Q}} - \lambda_{opt} \mathbf{I}_{NL})^{\dagger} \tilde{\mathbf{g}} = \tilde{\mathbf{x}}_{opt}. \quad (5.16)$$

When  $\lambda = \lambda_{min}$ ,  $\tilde{\mathbf{x}}_{opt}$  is the vector such that  $\|(\tilde{\mathbf{Q}} - \lambda_{opt} \mathbf{I}_{NL})\tilde{\mathbf{x}}_{opt} - \tilde{\mathbf{g}}\|_2^2$  is minimised [11, Theorem 19.7]. Hence, the optimisation problem can be solved by finding  $\lambda_{opt}$ .



### 5.3. Trade-off Design with a Total Power Constraint

First, assume that  $\lambda < \lambda_{min}$ , hence

$$\|h(\lambda)\|_2^2 = \|(\tilde{\mathbf{Q}} - \lambda \mathbf{I}_{NL})^{-1} \tilde{\mathbf{g}}\|_2^2, \quad (5.17)$$

since  $\tilde{\mathbf{Q}}$  is Hermitian, there exists an eigenvalue decomposition  $\mathbf{V}\mathbf{\Lambda}\mathbf{V}^H$ , where  $\mathbf{V}$  is a unitary matrix and  $\mathbf{\Lambda}$  is a real diagonal matrix consisting of the eigenvalues of  $\tilde{\mathbf{Q}}$  [11, Corollary 18.18]. Therefore, (5.17) can be rewritten as

$$\begin{aligned} \|h(\lambda)\|_2^2 &= \|(\mathbf{V}\mathbf{\Lambda}\mathbf{V}^H - \lambda \mathbf{I}_{NL})^{-1} \tilde{\mathbf{g}}\|_2^2 \\ &= \|(\mathbf{V}(\mathbf{\Lambda} - \lambda \mathbf{I}_{NL})\mathbf{V}^H)^{-1} \tilde{\mathbf{g}}\|_2^2 \\ &= \|\mathbf{V}(\mathbf{\Lambda} - \lambda \mathbf{I}_{NL})^{-1} \mathbf{V}^H \tilde{\mathbf{g}}\|_2^2. \end{aligned}$$

Since  $\mathbf{V}$  is a unitary matrix, it does not change the norm [11, Lemma 12.13]. Hence,

$$\begin{aligned} \|h(\lambda)\|_2^2 &= \|(\mathbf{\Lambda} - \lambda \mathbf{I}_{NL})^{-1} \mathbf{V}^H \tilde{\mathbf{g}}\|_2^2 \\ &= \sum_{i=1}^{NL} \frac{|(\mathbf{V}^H \tilde{\mathbf{g}})_i|^2}{(\lambda_i - \lambda)^2}, \end{aligned}$$

where  $\lambda_i$  is the  $i$ th smallest eigenvalue of  $\tilde{\mathbf{Q}}$ . It can be seen that  $\|h(\lambda)\|_2^2$  is a continuous and monotonically increasing function for  $\lambda < \lambda_{min}$ . Since  $\lambda_{opt} < \lambda_{min}$ , it must hold that  $\|h(\lambda_{opt})\|_2^2 < \|h(\lambda_{min})\|_2^2$ . Then, from (5.16) there must exist a unique  $\lambda_{opt} < \lambda_{min}$  satisfying (5.13) such that  $\lambda_{opt}$  is the root in

$$\|h(\lambda_{opt})\|_2^2 = \|\tilde{\mathbf{x}}_{opt}\|_2^2 = LP_T$$

[28, p. 4]. The root can be obtained by using a root finding algorithm such as the bisection method on the interval  $[a, \lambda_{min}]$ , where  $a < 0$  is chosen sufficiently small such that  $a < \lambda_{opt}$  [22, p. 148]. When  $\lambda_{opt}$  is obtained, we can find  $\mathbf{x}_{opt}$  by using (5.16).

The final algorithm for solving the optimisation problem for the trade-off design with a total power constraint can be seen in Algorithm 1.

---

#### Algorithm 1 Algorithm for Solving (5.8)

---

**Input:**  $\mathbf{H}, \mathbf{S}, \mathbf{X}_0, P_T$  and  $0 \leq \rho < 1$

**Output:**  $\mathbf{X}_{opt}$

1. Compute  $\tilde{\mathbf{g}}$  and  $\tilde{\mathbf{Q}}$ .
  2. Compute the eigenvalue decomposition  $\mathbf{V}\mathbf{\Lambda}\mathbf{V}^H$  of  $\tilde{\mathbf{Q}}$ .
  3. Find roots of  $\|h(\lambda)\|_2^2 - LP_T = 0$  on the interval  $[a, \lambda_{min}]$  using the bisection method.
  4. Compute  $\mathbf{x}_{opt} = (\tilde{\mathbf{Q}} - \lambda_{opt} \mathbf{I}_{NL})^\dagger \tilde{\mathbf{g}}$ .
  5. Reshape  $\mathbf{x}_{opt}$  into  $\mathbf{X}_{opt}$ .
- 

### The Hard Case

When  $\rho = 1$ , it is possible that we are in the hard case. Some known algorithms to solve this problem are the MS algorithm or the shift and deflation technique. These are presented in [28, p. 10] and [28, p. 33], respectively. However, since  $\rho = 1$ , communication is given full priority, and another waveform design focusing fully on communication might be preferable. Therefore, this problem will not be reviewed in this project.

## 6 Numerical Results

This chapter presents numerical results for the optimisation problems derived in Chapter 5. Various variables influence the numerical results. To centre the attention on the trade-off design the transmit power is set to  $P_T = 1$ , the number of antennas is  $N = 16$ , and the length of the communication frame is  $L = 30$ . However, the number of users,  $K$ , varies depending on the experiment.

The communication channel is assumed to be flat Rayleigh fading and is simulated as a standard complex Gaussian distribution, i.e.,  $H_{i,m} \sim \mathcal{CN}(0,1)$ . The transmitted symbols, encoded with a QPSK constellation, are drawn from a uniform distribution. For the radar system, the complex channel gain is modelled as a standard complex Gaussian distribution, i.e.,  $\beta_b \sim \mathcal{CN}(0,1)$ . The false alarm probability is set to  $P_{FA} = 10^{-3}$ .

The signal-to-noise ratio (SNR) at the users, referred to as the communication SNR, is defined as

$$SNR_{com} = \frac{P_T}{N_0}.$$

The SNR at the radar receiver is referred to as the radar SNR and is defined as

$$SNR_{rad} = \frac{P_T}{\sigma_\epsilon^2}.$$

Having specified the assumptions for the numerical experiments, our results will be presented.

### 6.1 Omnidirectional and Directional Beampatterns with Strict Equalities

For this section, we first show the transmit beampattern for the omnidirectional and directional beampattern designs with strict equality constraints, as derived in Section 5.1 and Section 5.2, respectively. The omnidirectional and directional beampattern are depicted in Figure 6.1.

### 6.1. Omnidirectional and Directional Beampatterns with Strict Equalities

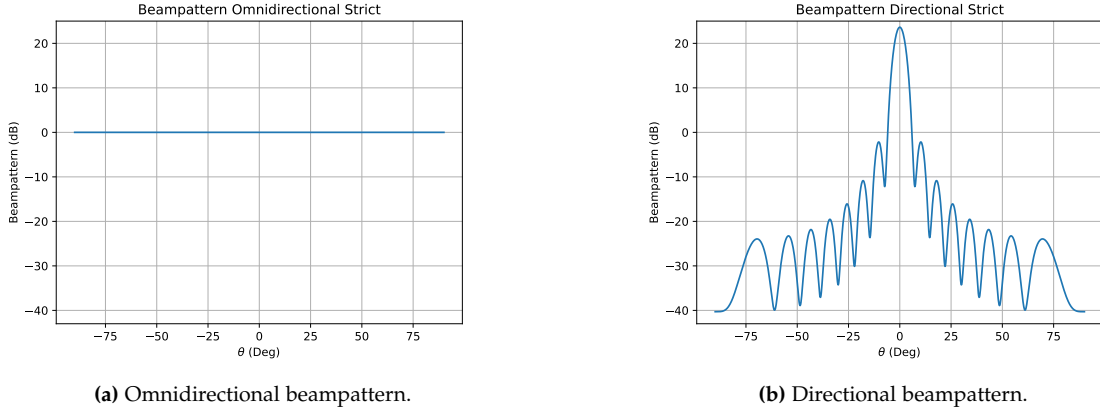


**Figure 6.1:** Beampatterns for the omnidirectional and directional waveforms.

In Figure 6.1a, the beampattern is seen to be evenly distributed, which is desired for the omnidirectional beampattern. In Figure 6.1b, we consider one target at  $\theta = 0^\circ$ . It can be seen that the transmit power is concentrated at  $\theta = 0^\circ$ , which is desired for the directional beampattern.

To show the communication performance, the SEP is plotted as a function of  $SNR_{com}$  in Figure 6.2.

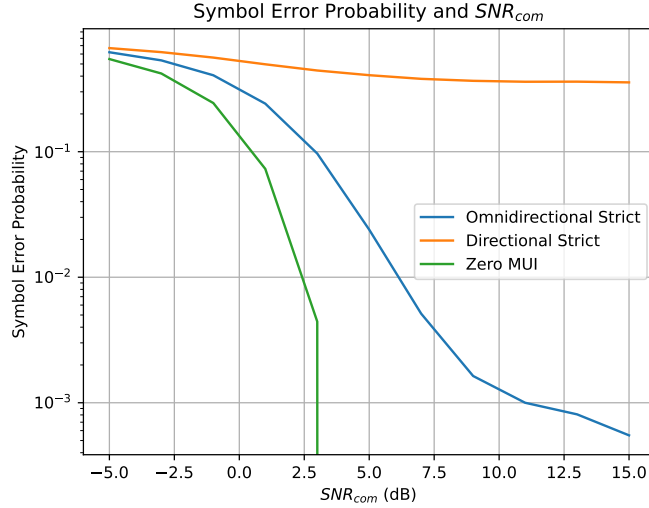


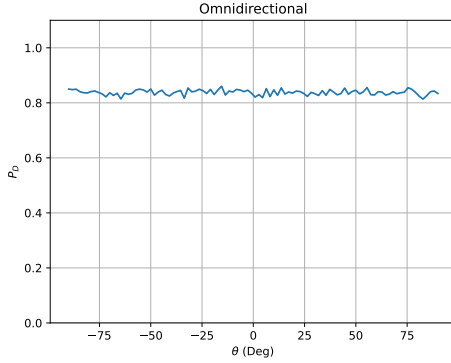
**Figure 6.2:** SEP comparison.

In Figure 6.2, it can be seen that the omnidirectional waveform outperforms the directional waveform. This is due to the directional waveform focusing only in one direction. Therefore, when the  $SNR_{com}$  increases, the SEP only decreases a little. Compared to the omnidirectional waveform, which transmits equally in all directions, the SEP is constant in all directions, so as the  $SNR_{com}$  increases, the SEP will decrease more. Furthermore, the zero MUI is a theoretical minimum, i.e.,  $\mathbf{H}\mathbf{X} - \mathbf{S} = \mathbf{0}$ , thus  $\mathbf{Y}_{com} = \mathbf{S} + \mathbf{W}$  with is a

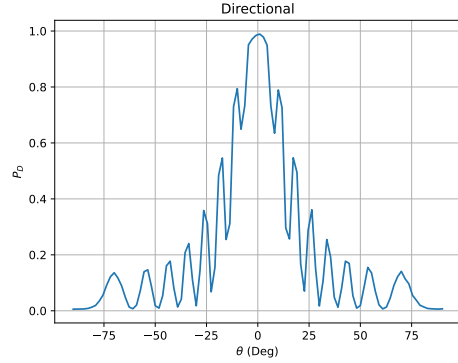
### 6.1. Omnidirectional and Directional Beampatterns with Strict Equalities

Gaussian channel. Therefore, as the  $SNR_{com}$  increases, the SEP decreases until only a signal is present. Both the omnidirectional and directional waveforms are far away from the theoretical minimum. Especially the directional waveform has poor performance in terms of the SEP.

In Figure 6.3, the detection probability  $P_D$  is plotted as a function of the angle  $\theta$  with  $SNR_{rad} = -8$  dB.



(a) Detection probability  $P_D(\theta)$  for the omnidirectional waveform with  $SNR_{rad} = -8$  dB.



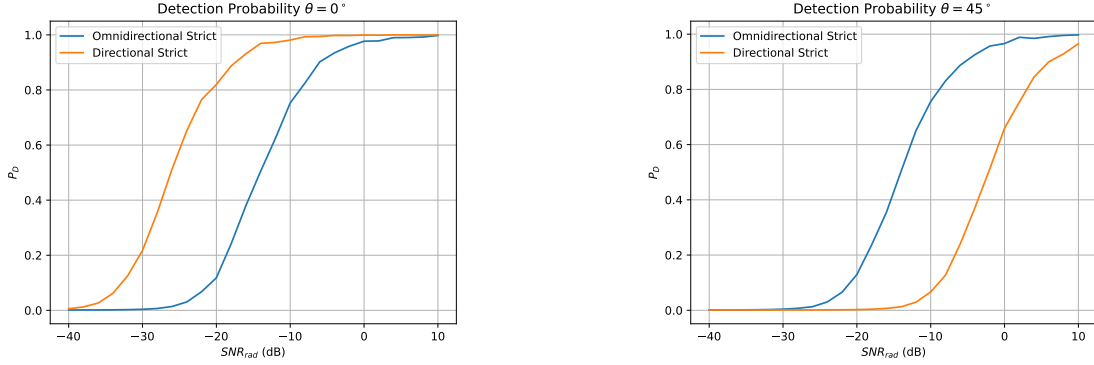
(b) Detection probability  $P_D(\theta)$  for the directional waveform with  $SNR_{rad} = -8$  dB.

**Figure 6.3:** Detection probability for the omnidirectional and directional waveform.

For the omnidirectional waveform in Figure 6.3a, the detection probability is evenly distributed over all possible angles of  $\theta$ . For the directional waveform in Figure 6.3b, the detection probability is concentrated at  $\theta = 0^\circ$ , where the detection probability almost reach 100%. The further away the angles are from  $\theta = 0^\circ$ , the lower the detection probability becomes. Therefore, if the target is placed at  $\theta = 0^\circ$ , the directional waveform is preferred since it has a higher detection probability at that angle. However, if the target's position is further away from  $\theta = 0^\circ$ , the omnidirectional waveform is preferred since it has a detection probability over 80% for all angles.

### 6.1. Omnidirectional and Directional Beampatterns with Strict Equalities

The  $SNR_{rad}$  affects the detection probability. This can be seen in Figure 6.4.



(a) Detection probability  $P_D(\theta)$  and  $SNR_{rad}$  for  $\theta = 0^\circ$ .

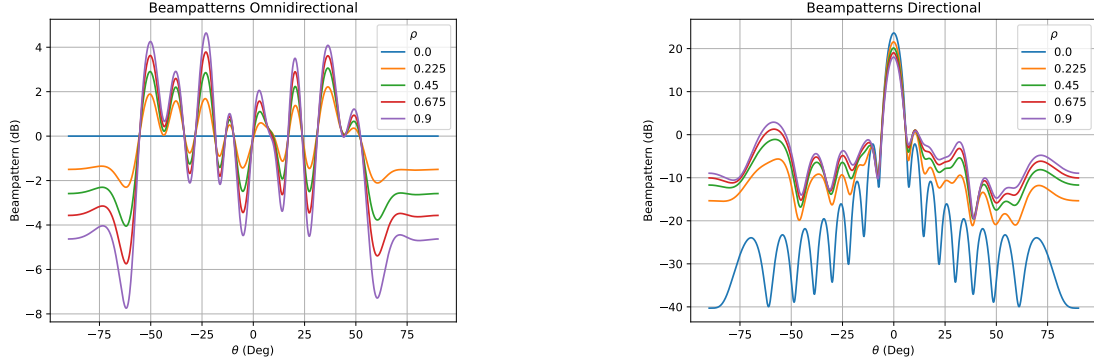
(b) Detection probability  $P_D(\theta)$  and  $SNR_{rad}$  for  $\theta = 45^\circ$ .

**Figure 6.4:** Detection probability for the omnidirectional and directional waveforms with different angles.

In Figure 6.4a, the detection probability increases faster for the directional than for the omnidirectional waveform. For  $SNR_{rad} = -30$  dB, the directional waveform has a detection probability over 20%, whereas the omnidirectional still has a detection probability close to 0% at the same  $SNR_{rad}$ . The directional waveform reaches a detection probability of over 80% at an  $SNR_{rad}$  value more than 10 dB smaller than the  $SNR_{rad}$  value where the omnidirectional waveform obtains the same detection probability. Therefore, it is clearly observed that the directional waveform outperforms the omnidirectional. However, note that in the figure,  $\theta = 0^\circ$ , which is where the directional waveform is concentrated. Therefore, the directional waveform is expected to perform better than the omnidirectional. In Figure 6.4b, the opposite happens, i.e., the omnidirectional waveform outperforms the directional. In this case,  $\theta = 45^\circ$ . Therefore, the outcome in the figure is expected since the directional waveform is concentrated at  $\theta = 0^\circ$ .

## 6.2 Trade-off with a Total Power Constraint

The beampatterns for the trade-off design with a total power constraint, as derived in Section 5.3, are plotted in Figure 6.5 for  $K = 4$ . The waveform  $\mathbf{X}_0$  is the waveform derived for the omnidirectional, Section 5.1, or directional beampattern, Section 5.2, with a strict equality constraint and using  $a = -2$  to finding a root in Algorithm 1.



(a) Omnidirectional beampatterns for different values of  $\rho$ .

(b) Directional beampatterns for different values of  $\rho$ .

**Figure 6.5:** Beampatterns for different values of  $\rho$ . The channel matrix and symbol matrix is constant.

In Figure 6.5a, the omnidirectional beampatterns for different values of  $\rho$  are plotted. When  $\rho = 0$ , the beampattern is identical to the one in Figure 6.1a for the omnidirectional with a strict equality constraint, as expected. As  $\rho$  increases, so do the fluctuations in the beampatterns. Therefore, the order of the beampatterns is constant for the different values of  $\rho$ . The beampattern for  $\rho = 0.9$  has always bigger fluctuations than any of the beampatterns for smaller values of  $\rho$ . In the same way, for  $\rho = 0.225$ , the beampattern has always smaller fluctuations than any of the beampatterns for higher values of  $\rho$ . This outcome of the beampatterns is expected since for higher values of  $\rho$ , the beampatterns deviate more from the initial radar beampattern.

The directional beampatterns for different values of  $\rho$  are plotted in Figure 6.5b. When  $\rho = 0$ , the beampattern is identical to Figure 6.1b for the directional with a strict equality constraint. As  $\rho$  increases, the beampatterns become more efficient for communication since the energy is more evenly distributed over the different angles. However, for  $\rho = 0.9$ , the beampattern is still very concentrated at  $\theta = 0^\circ$ .

### Omnidirectional Trade-off

Different plots for the omnidirectional trade-off waveform are presented in Figure 6.6 for  $K = 4$ .

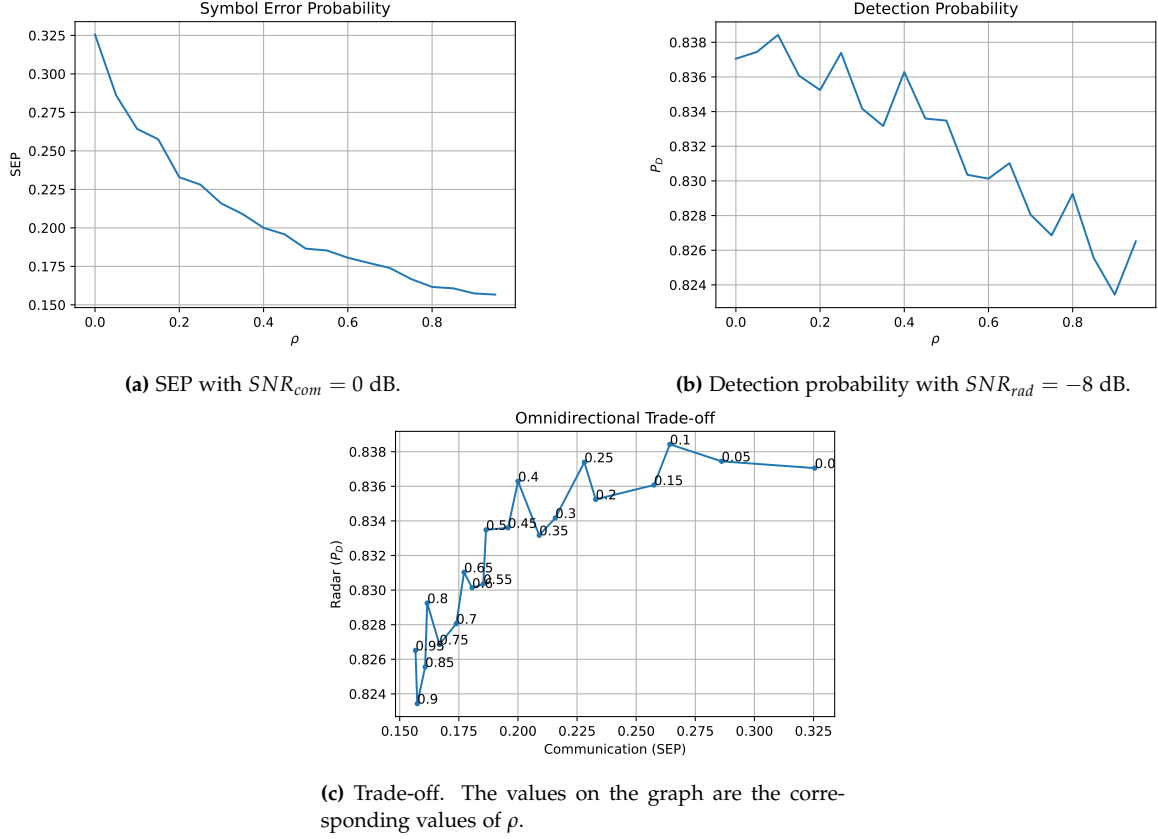


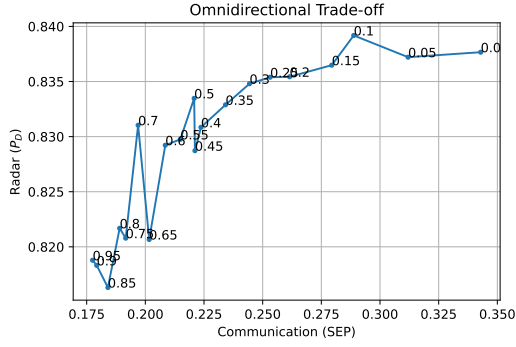
**Figure 6.6:** Plots for the omnidirectional waveform trade-off design with  $K = 4$ .

The SEP is plotted in Figure 6.6a for different values of  $\rho$ . For  $\rho = 0$ , the SEP is 32.5%. However, a high SEP is expected for small values of  $\rho$ , since radar is given full priority when  $\rho = 0$ . Therefore, as  $\rho$  increases, the SEP decreases as expected. In Figure 6.6b, the detection probability is plotted for different values of  $\rho$ . The detection probability decreases for higher values of  $\rho$ , which is expected since the communication is given full priority at  $\rho = 1$ . The spikes occurs due to the small change in detection probability on the  $y$ -axis.

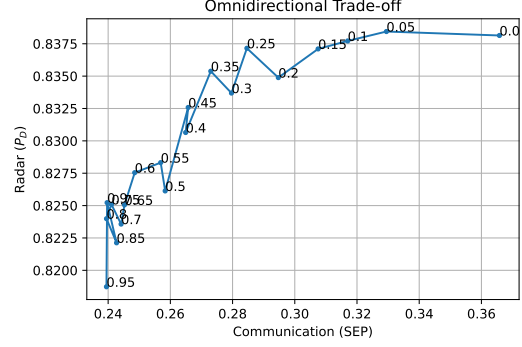
The trade-off between radar and communication for the omnidirectional waveform is illustrated on Figure 6.6c for different values of  $\rho$ . When  $\rho$  is close to zero, the detection probability increases, which enhances radar performance. At the same time, the SEP also increases, leading to degraded communication performance. When  $\rho$  is close to 1, the opposite happens, meaning that both the detection probability and SEP decrease. This leads to enhanced communication performance and degraded radar performance. Therefore, the trade-off plot confirms that the performance balance between radar and communication is controlled by  $\rho$ .

## 6.2. Trade-off with a Total Power Constraint

In Figure 6.7, the trade-off plots are generated for  $K = 6$  and  $K = 8$ .



(a)  $K = 6$ .



(b)  $K = 8$ .

**Figure 6.7:** Plots for the omnidirectional waveform trade-off design at  $\theta = 0^\circ$ . The  $SNR_{com} = 0$  dB and  $SNR_{rad} = -8$  dB. The values on the graphs are the corresponding values of  $\rho$ .

In both Figure 6.7a and Figure 6.7b, there is a small decrease in the detection probability for large values of  $\rho$  compared to Figure 6.6c. Furthermore, there is an increase in the SEP for more users. For  $\rho = 0.95$  in Figure 6.6c, the SEP is approximately 15%, whereas in Figure 6.7b, the SEP is close to 25% for the same value of  $\rho$ . This is due to an increase in the number of users, which causes more interference.



## 6.2. Trade-off with a Total Power Constraint

### Directional Trade-off

Different plots for the directional trade-off waveform are presented in Figure 6.8 for  $K = 4$ .

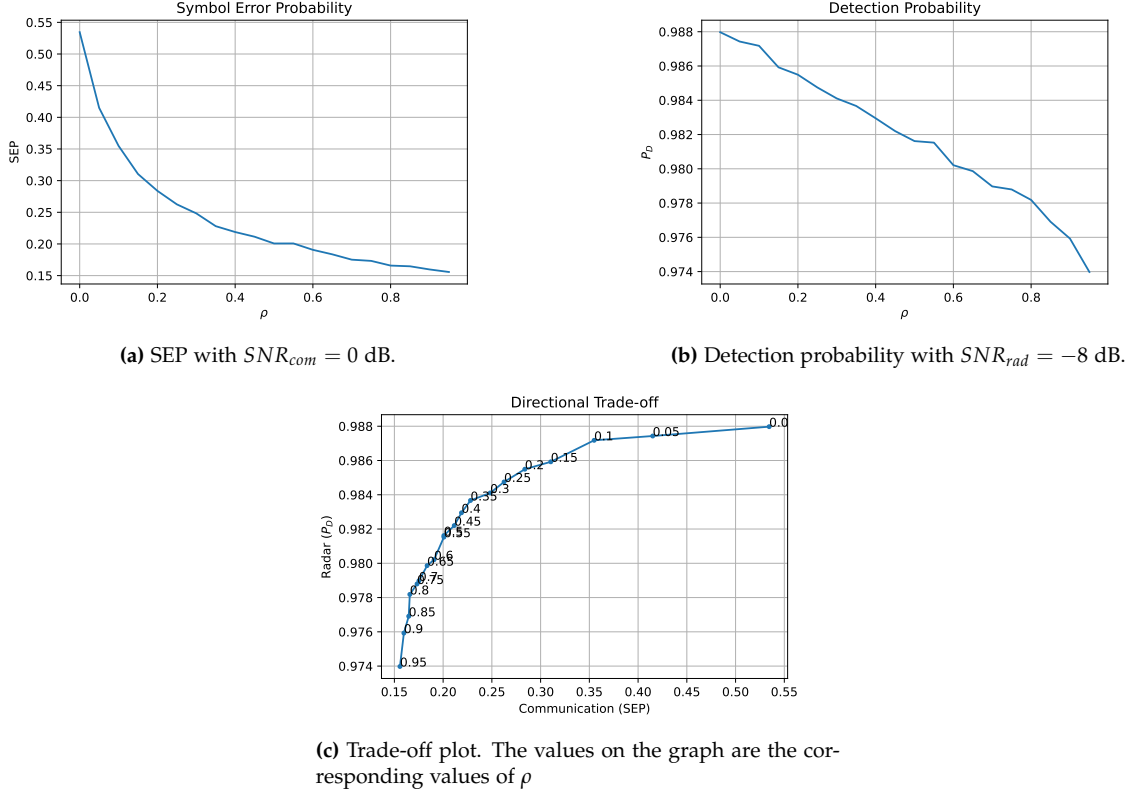


**Figure 6.8:** Plots for the directional waveform trade-off design at  $\theta = 0^\circ$  with  $K = 4$ .

The SEP and detection probability for different values of  $\rho$  are plotted in Figure 6.8a and Figure 6.8b, respectively. Both plots show the same tendencies as in the case with the omnidirectional waveform. As  $\rho$  increases, the SEP and detection probability decrease, as expected. However, the SEP for  $\rho = 0$  is more than 50% compared to the omnidirectional waveform, where the SEP was 32.5% for the same value of  $\rho$  and  $K = 4$ . This occurs since the directional waveform has a more degraded communication performance at  $\rho = 0$  compared to the omnidirectional waveform due to the power being concentrated at  $\theta = 0^\circ$ . The detection probability for  $\rho = 0$  is more than 15% higher compared to the omnidirectional waveform for the same value of  $\rho$  and  $K = 4$ . This is a leap in the radar's performance due to the directional waveform having increased detection probability at  $\theta = 0^\circ$ .

In Figure 6.8c the trade-off between the radar and communication is plotted. The observations are the same as in the case for the omnidirectional waveform. However, the detection probability and SEP are increased, as explained previously.

## 6.2. Trade-off with a Total Power Constraint

The trade-off plots are generated for  $K = 6$  and  $K = 8$  in Figure 6.9.

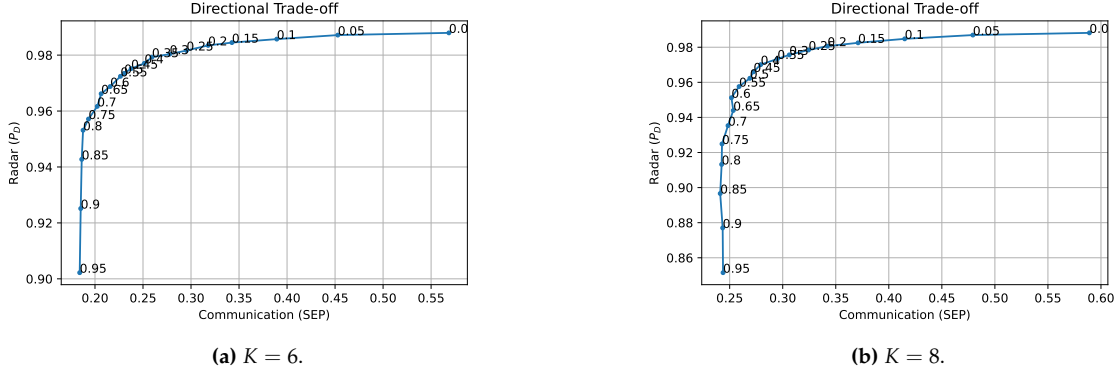


**Figure 6.9:** Plots for the directional waveform trade-off design at  $\theta = 0^\circ$ . The  $SNR_{com} = 0$  dB and  $SNR_{rad} = -8$  dB. The values on the graphs are the corresponding values of  $\rho$ .

In Figure 6.9a for  $\rho = 0.95$ , the detection probability drops to almost 90% in comparison to 97.4% for the same value of  $\rho$  when  $K = 4$  in Figure 6.8c. The decrease is due to more users increasing the demand for better communication performance. The trade-off is a lower radar performance. Furthermore, there is an increase in the SEP, which is expected as more users interfere with each other. For  $K = 8$  in Figure 6.9b, the same tendency is observed.

## Comparisons

On Figure 6.10, the SEP and detection probability are plotted for the omnidirectional and directional waveforms with strict equalities and a trade-off design with  $\rho = 0.5$ . These are shown as a function of SNR.

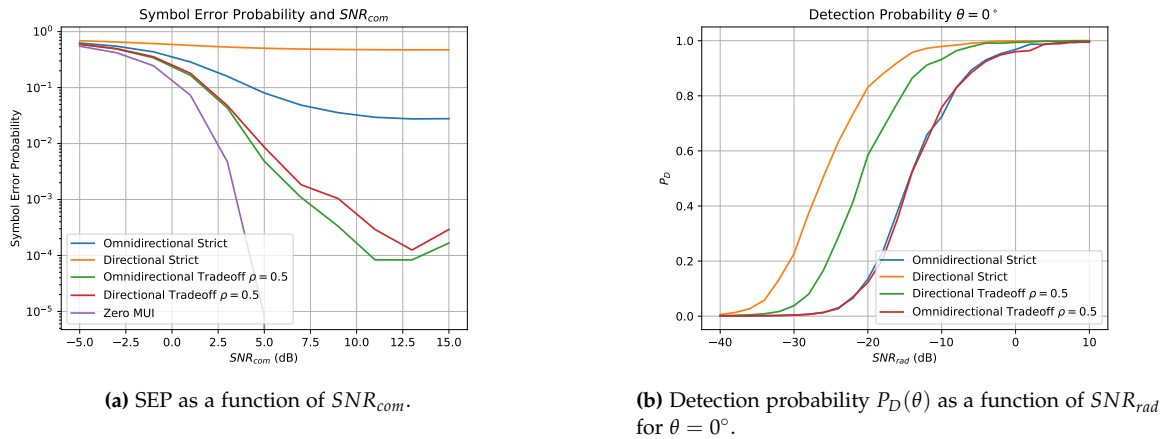


**Figure 6.10:** Comparison between omnidirectional and directional waveforms with strict equalities and trade-off design with  $\rho = 0.5$ .  $K = 8$ .

## 6.2. Trade-off with a Total Power Constraint

In Figure 6.10a, it can be seen that for both the omnidirectional and directional trade-off designs with  $\rho = 0.5$  the SEP decreases compared to their respective waveforms with strict equalities. This leads to an enhanced communication performance. The detection probability for the different waveforms is plotted in Figure 6.10b. The directional waveform design entails a decrease in the detection probability for the trade-off design with  $\rho = 0.5$  compared to the directional waveform with strict equality. This illustrates the trade-off where a decrease in SEP entails a decrease in detection probability. For the omnidirectional waveform, the detection probability remains almost unchanged for the trade-off and strict equality designs.

## 7 Discussion

In this project, our purpose was to design a dual-functional waveform with an adjustable trade-off between sensing and communication performance. Therefore, a technique to design such a waveform has been derived. Numerical results were presented to examine the efficiency of the technique for an adjustable trade-off.

The derived technique encountered a problem when the weighting factor for the radar and communication performance was equal to  $\rho = 1$ . This was considered a possible hard case. However, when  $\rho = 1$ , the communication part of the system was given full priority, and one might be interested in designing a waveform fully intended for communication. Therefore, this case was disregarded in this project since our focus was on designing an adjustable trade-off.

In Section 6.2, we found that the detection probability decreased as the SEP decreased for both the omnidirectional and directional waveform. This confirms that we have obtained an adjustable trade-off between sensing and communication performance, where one is reinforced at the expense of the other. For the omnidirectional, waveform there was only a small decrease in the detection probability. Therefore, it was possible to enhance the communication performance significantly without losing a lot of radar performance. For the directional waveform, there was a larger decrease in the detection probability compared to the omnidirectional waveform. Although it was still considered a small decrease. To be able to specify further when a decrease in the detection probability is small or large, one could, for instance, introduce a desired threshold for the detection probability depending on their objective.

## 8 Conclusion

A key feature in 6G will be a dual-functional RadCom waveform. In this project, a dual-functioning waveform design with an adjustable trade-off between sensing and communication performance has therefore been derived.

First, a narrowband communication model was presented, and the Rayleigh fading channel model was developed. The SEP was presented as a metric for communication performance. Next, a model of MIMO radar was modelled and a technique for designing both omnidirectional and directional probing signals was presented. The detection probability was derived as a metric for the radar performance. In order to design the waveform, two optimisation methods were presented: the orthogonal Procrustes problem and the TRS. The orthogonal Procrustes problem was then used to design a waveform minimising the MUI energy for an omnidirectional and directional beampattern. Next, the TRS was used to design a waveform with an adjustable trade-off between minimising the MUI energy and a desired radar waveform under a total power constraint. Lastly, the numerical results were presented in order to validate the performance of the waveform.

To conclude, a technique to design a dual-functional waveform with an adjustable trade-off has been developed. The technique in this project does not take into account the case where the communication part is fully prioritised. The designed dual-functional waveform achieved an adjustable trade-off between radar and communication performance.

# Bibliography

- [1] Zohair Abu-Shaban et al. "Error Bounds for Uplink and Downlink 3D Localization in 5G Millimeter Wave Systems". In: *IEEE Transactions on Wireless Communications* 17.8 (2018), pp. 4939–4954.
- [2] Mahdi Boloursaz Mashhadi and Deniz Gündüz. "Deep Learning for Massive MIMO Channel State Acquisition and Feedback". In: *Journal of the Indian Institute of Science* (2020), pp. 369–382.
- [3] Stephen Boyd and Lieven Vandenberghe. *Convex Optimization*. Cambridge University Press, 2004. ISBN: 9780521833783.
- [4] Emilio Calvanese Strinati et al. "Wireless Environment as a Service Enabled by Reconfigurable Intelligent Surfaces: The RISE-6G Perspective". In: *6G Enabling Technologies* (2021), pp. 562–567.
- [5] Charles Fortin. "A Survey of the Trust Region Subproblem Within a Semidefinite Framework". PhD thesis. University of Waterloo, 2000.
- [6] Noor Hidayah Muhamad Adnan, Islam Md. Rafiqul, and AHM Zahirul Alam. "Effects of Inter Element Spacing on Large Antenna Array Characteristics". In: *IEEE International Conference on Smart Instrumentation, Measurement and Applications* (2017), pp. 1–5.
- [7] Sai Huang et al. "MIMO Radar Aided mmwave Time-Varying Channel Estimation in MU-MIMO V2X Communications". In: *IEEE Transactions on Wireless Communications* 20.11 (2021), pp. 7581–7594.
- [8] Morten Lomholt Jakobsen. "Modeling and Estimation of Wireless Multipath Channels". PhD thesis. Master's thesis, Aalborg University, 2009.
- [9] Hamid Krim and Mats Viberg. "Two Decades of Array Signal Processing Research: The Parametric Approach". In: *IEEE signal processing magazine* 13.4 (1996), pp. 67–94.
- [10] Jian Li and Petre Stoica. *MIMO Radar Signal Processing*. Wiley, 2009. ISBN: 9780470178980.
- [11] Jörg Liesen and Volker Mehrmann. *Linear Algebra*. Springer, 2015. ISBN: 9783319243443.
- [12] Fan Liu et al. "Integrated Sensing and Communications: Toward Dual-Functional Wireless Networks for 6G and Beyond". In: (2022). Last accessed 20 February 2023. URL: <https://ieeexplore.ieee.org/document/9737357>.
- [13] Fan Liu et al. "Toward Dual-Functional Radar-Communication Systems: Optimal Waveform Design". In: *IEEE Transactions on Signal Processing* 66.16 (2018), pp. 4264–4279.
- [14] Carl D Meyer. *Matrix Analysis and Applied Linear Algebra*. Vol. 71. Siam, 2000. ISBN: 0898714540.

## Bibliography

- [15] Saif Khan Mohammed and Erik G Larsson. "Per-antenna Constant Envelope Precoding for Large Multi-User MIMO Systems". In: *IEEE Transactions on Communications* 61.3 (2013), pp. 1059–1071.
- [16] Petar Popovski. *Wireless Connectivity: An Intuitive and Fundamental Guide*. John Wiley & Sons, 2020. ISBN: 9780470683996.
- [17] John G Proakis and Masoud Salehi. *Digital Communications*. 5th edition. McGraw-Hill Book Company, 2001. ISBN: 9780072957167.
- [18] Daniel R. Fuhrmann and Geoffrey San Antonio. "Transmit Beamforming for MIMO Radar Systems using Signal Cross-Correlation". In: *IEEE Transactions on Aerospace and Electronic Systems* 44.1 (2008), pp. 171–186.
- [19] Merrill Skolnik. *Introduction to Radar Systems*. 1. edition. McGraw-Hill Book Company, 1980. ISBN: 0-07066572-9.
- [20] David Tse and Pramod Viswanath. *Fundamentals of Wireless Communication*. Cambridge University Press, 2005. ISBN: 9780521845274.
- [21] George Turin. "An introduction to Matched Filters". In: *IRE transactions on Information theory* 6.3 (1960), pp. 311–329.
- [22] Peter R Turner, Thomas Arildsen, and Kathleen Kavanagh. *Applied Scientific Computing: With Python*. Springer, 2018. ISBN: 9783319895741.
- [23] Thomas Viklands. "Algorithms for the Weighted Orthogonal Procrustes Problem and Other Least Squares Problems". PhD thesis. Umeå University, 2006.
- [24] Robert W. Health Jr. et al. "An Overview of Signal Processing Techniques for Millimeter Wave MIMO Systems". In: *IEEE Journal of Selected Topics in Signal Processing* 10.3 (2016), pp. 436–453.
- [25] Ai-Guo Wu and Ying Zhang. *Complex Conjugate Matrix Equations for Systems and Control*. Springer, 2017. ISBN: 9789811006357.
- [26] Yulei Wu et al. *6G Mobile Wireless Networks*. Springer, 2021. ISBN: 9783030727765.
- [27] Henk Wymeersch and Gonzalo Seco-Granados. "Adaptive Detection Probability for mmWave 5G SLAM". In: *2020 2nd 6G Wireless Summit (6G SUMMIT)*. IEEE. 2020, pp. 1–5.
- [28] Heng Ye. "Efficient Trust Region Subproblem Algorithms". MA thesis. University of Waterloo, 2011.

# A Linear Algebra

## Definition A.1 (Trace of a Matrix)

The trace of a matrix  $\mathbf{A} \in \mathbb{C}^{n \times n}$ , denoted  $\text{Tr}(\mathbf{A})$ , is defined as the sum of the diagonal entries of  $\mathbf{A}$ . It is written as

$$\text{Tr}(\mathbf{A}) = \sum_{i=1}^n a_{i,i}.$$

[14, p. 90]

## Lemma A.2 (Trace of Matrix Product)

If  $\mathbf{A} \in \mathbb{C}^{m \times n}$  and  $\mathbf{B} \in \mathbb{C}^{n \times m}$ , then

$$\text{Tr}(\mathbf{AB}) = \text{Tr}(\mathbf{BA}).$$

[14, p. 110]

## Proof

Let  $\mathbf{A} = [a_{k,i}]$  and  $\mathbf{B} = [b_{k,i}]$ , then the  $i$ 'th term on the diagonal of  $\mathbf{AB}$  equals

$$\sum_{k=1}^n a_{i,k} b_{k,i}.$$

Thus

$$\begin{aligned} \text{Tr}(\mathbf{AB}) &= \sum_{i=1}^n [\mathbf{AB}]_{i,i} \\ &= \sum_{i=1}^n \sum_{k=1}^n a_{i,k} b_{k,i} \\ &= \sum_{k=1}^n \sum_{i=1}^n b_{k,i} a_{i,k} \\ &= \sum_{k=1}^n [\mathbf{BA}]_{k,k} \\ &= \text{Tr}(\mathbf{BA}) \end{aligned}$$

as desired. ■

Lemma A.2 can be extended to show that the trace is invariant under cyclic permutation. This is called the cyclic property of trace, for any conformable matrix product

$$\text{Tr}(\mathbf{ABC}) = \text{Tr}(\mathbf{BCA}) = \text{Tr}(\mathbf{CAB}).$$



Noncyclic or arbitrary permutations does not preserve the trace, such as

$$\text{Tr}(\mathbf{ABC}) \neq \text{Tr}(\mathbf{BAC}).$$

**Lemma A.3**

If  $\mathbf{A} \in \mathbb{C}^{n \times n}$  then

$$\text{Tr}(\mathbf{A}^H) = \overline{\text{Tr}(\mathbf{A})}$$

**Proof**

Let  $\mathbf{A} \in \mathbb{C}^{n \times n}$  then

$$\begin{aligned} \text{Tr}(\mathbf{A}^H) &= \sum_{i=1}^n \overline{a_{i,i}} \\ &= \overline{\sum_{i=1}^n a_{i,i}} \\ &= \overline{\text{Tr}(\mathbf{A})}. \end{aligned}$$

■

**Definition A.4 (Frobenius Matrix Norm)**

The Frobenius norm of  $\mathbf{A} \in \mathbb{C}^{m \times n}$  is defined by the equations

$$\|\mathbf{A}\|_F^2 = \sum_i \sum_k |a_{i,k}|^2 = \text{Tr}(\mathbf{A}^H \mathbf{A}).$$

[14, p. 279]

**Lemma A.5**

If  $\mathbf{A}$  is a Hermitian matrix, then  $\mathbf{x}^H \mathbf{A} \mathbf{x}$  is real valued.

[25, Lemma 11.1]

**Proof**

If  $\mathbf{A}$  is a Hermitian matrix, then  $\mathbf{A}^H = \mathbf{A}$ . Finding the conjugate transpose of the expression  $\mathbf{x}^H \mathbf{A} \mathbf{x}$  yields

$$(\mathbf{x}^H \mathbf{A} \mathbf{x})^H = \mathbf{x}^H \mathbf{A}^H \mathbf{x} = \mathbf{x}^H \mathbf{A} \mathbf{x}.$$

Since the conjugate transpose of the expression yields itself, the expression must be real valued. ■